J|A|C|S
ARTICLES
Published on Web 04/11/2006

Anion−π Interactions as Controlling Elements in Self-Assembly Reactions of Ag(I) Complexes with π-Acidic Aromatic Rings

Brandi L. Schottel,[†] Helen T. Chifotides,[†] Mikhail Shatruk,[†] Abdellatif Chouai,[†] Lisa M. Pérez,[†,§] John Bacsa,[†] and Kim R. Dunbar*[,†]

Contribution from the Department of Chemistry and Laboratory for Molecular Simulation, Texas A&M University, P.O. Box 30012, College Station, Texas 77842-3012

Received January 26, 2006; E-mail: dunbar@mail.chem.tamu.edu

Abstract: Reactions of 3,6-bis(2′-pyridyl)-1,2,4,5-tetrazine (bptz) and 3,6-bis(2′-pyridyl)-1,2-pyridazine (bppn) with the AgX salts (X = $[PF_6]^-$, $[AsF_6]^-$, $[SbF_6]^-$, and $[BF_4]^-$) afford complexes of different structural motifs depending on the π-acidity of the ligand central ring and the outer-sphere anion. The bptz reactions lead to the polymeric $\{[Ag(bptz)][PF_6]\}_\infty$ (**1**) and the dinuclear compounds $[Ag_2(bptz)_2(CH_3CN)_2][PF_6]_2$ (**2**) and $[Ag_2(bptz)_2(CH_3CN)_2][AsF_6]_2$ (**3**), as well as the propeller-type species $[Ag_2(bptz)_3][AsF_6]_2$ (**4**) and $[Ag_2(bptz)_3][SbF_6]_2$ (**5a** and **5b**). Reactions of bppn with AgX produce the grid-type structures $[Ag_4(bppn)_4][X]_4$ (**6**−**9**), regardless of the anion present. In **6**−**9**, $\pi-\pi$ stacking interactions are maximized, whereas multiple and shorter (therefore stronger) anion−π interactions between the anions and the tetrazine rings are established in **1**−**5b**. These differences reflect the more electron-rich character of the bppn pyridazine ring as compared to the bptz tetrazine ring. The evidence gleaned from the solid-state structures was corroborated by density functional theory calculations. In the electrostatic potential maps of the free ligands, a higher positive charge is present in the bptz as compared to the bppn central ring. Furthermore, the electrostatic potential maps of **3**, **4**, and **5b** indicate an electron density transfer from the anions to the π-acidic rings. Conversely, upon addition of the $[AsF_6]^-$ ions to the cation of **7**, there is negligible change in the electron density of the central pyridazine ring, which supports the presence of weaker anion−π interactions in the bppn as compared to the bptz complexes. From the systems studied herein, it is concluded that anion−π interactions play an important role in the outcome of self-assembly reactions.

Introduction

Supramolecular chemistry, the chemistry of noncovalent interactions, is one of the most active research areas at the forefront of chemistry and biology.[1−3] The roots of supramolecular chemistry can be traced back to Pedersen's report of cation-encapsulating crown ethers[4] and Lehn's account of the first cryptate.[5] In the ensuing decades since these early accounts, supramolecular host−guest compounds involving neutral or cationic entities have received considerable attention. In sharp contrast, noncovalent interactions of anions have been much less appreciated, despite the report of the first example of an encapsulated anion system[6] during the nascence of supramolecular chemistry. Since the work of Hawthorne et al. beginning a decade ago,[7] however, reports of the role of anions in the self-assembly of transition metal complexes have increased,[8,9] although there are still far fewer examples in comparison to analogous studies involving cations. It is considerably more challenging to design molecules templated by anions as compared to cation-assisted processes,[10] a fact that can be attributed to anions' larger size as compared to cations, their wide range of coordination geometries, their much higher free energies of solvation, and their electronic "saturation".[8,9,11]

Numerous examples of cation−π interactions in many organic and biochemical systems have been reported,[12,13] but the electron-donating character of anions and the expected repulsive interactions with aromatic π-systems have limited the development of noncovalent anion−π interaction chemistry. A few NMR studies, however, indicate association between neutral π-moieties and negatively charged groups,[14−18] and several

[†] Department of Chemistry.
[§] Laboratory for Molecular Simulation.

(1) Leininger, S.; Olenyuk, B.; Stang, P. J. *Chem. Rev.* **2000**, *100*, 853.
(2) Lehn, J.-M. *Supramolecular Chemistry: Concepts and Perspectives*; VCH: Weinheim 1995.
(3) Steed, J. W.; Atwood, J. L. *Supramolecular Chemistry*; John Wiley: New York, 2001.
(4) Pedersen, C. J. *J. Am. Chem. Soc.* **1967**, *89*, 7017.
(5) Dietrich, B.; Lehn, J. M.; Sauvage, J. P. *Tetrahedron Lett.* **1969**, *34*, 2889.
(6) Park, C. H.; Simmons, H. E. *J. Am. Chem. Soc.* **1968**, *90*, 2431.
(7) (a) Yang, X.; Knobler, C. B.; Zheng, Z.; Hawthorne, M. F. *J. Am. Chem. Soc.* **1994**, *116*, 7142. (b) Hawthorne, M. F.; Yang, X.; Zheng, Z. *Pure Appl. Chem.* **1994**, *66*, 245. (c) Lee, H.; Diaz, M.; Knobler, C. B.; Hawthorne, M. F. *Angew. Chem.* **2000**, *112*, 792.
(8) Vilar, R. *Angew. Chem., Int. Ed.* **2003**, *42*, 1460.
(9) Beer, P. D.; Gale, P. A. *Angew. Chem., Int. Ed.* **2001**, *40*, 486 and references therein.
(10) Atwood, J. L. Structural and Topological Aspects of Anion Coordination. In *Supramolecular Chemistry of Anions*; Bianchi, A., Bowman-James, K., García-España, E., Eds.; John Wiley-VCH: New York, 1997; p 147.
(11) Bianchi, A.; García-España, E. Thermodynamics of Anion Complexation. In *Supramolecular Chemistry of Anions*; Bianchi, A., Bowman-James, K., García-España, E., Eds.; Wiley-VCH: New York, 1997; pp 217−275.
(12) Meyer, E. A.; Castellano, R. K.; Diederich, F. *Angew. Chem., Int. Ed.* **2003**, *42*, 1210.
(13) Ma, J. C.; Dougherty, D. A. *Chem. Rev.* **1997**, *97*, 1303.

Chart 1

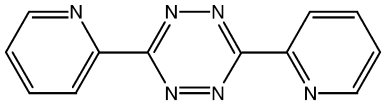

bptz

theoretical studies suggest that noncovalent electrostatic interactions between anions and π-electron-deficient aromatic rings (i.e., hexafluorobenzene, trinitrobenzene, *s*-triazine, and *s*-tetrazine), primarily consisting of electrostatic and anion-induced polarization contributions,[19g,i] are energetically favorable.[19−24] Recently, the term "anion$-\pi$ interaction" was coined by Frontera et al. to describe these interactions.[19a] Crystallographic evidence of their existence in the solid state, suggested by the proximity of the anions to the π-acidic ring systems, has been obtained in several cases.[18,25−30] Upfield ^{19}F NMR shifts[17a] of the fluorine atoms and unusually high association constants between the anion and the C_6F_5 aromatic system[17b] in C_6F_5-substituted *N*-confused porphyrins have been attributed to anion$-\pi$ interactions as well. Interest in the nature of these interactions stems from the potential use of electron-deficient aryl hosts as molecular receptors for the recognition of anions with important biological and medicinal applications.[19k,l,20,27]

Previous studies conducted in our laboratories with the bis-bidentate bipyridine ligand 3,6-bis(2′-pyridyl)-1,2,4,5-tetrazine (bptz; Chart 1) and divalent metal ions provide compelling evidence that the anions play a decisive role in the formation of a particular cyclic structure both in the solid state and in solution. In the case of Ni(II), the tetrahedral anions $[BF_4]^-$ and $[ClO_4]^-$ act as templates for the formation of molecular squares $[Ni_4(bptz)_4(CH_3CN)_8\subset X][X]_7$ ($X = [BF_4]^-$, $[ClO_4]^-$),[31] whereas the anion $[SbF_6]^-$ leads to the exclusive formation of the molecular pentagon $[Ni_5(bptz)_5(CH_3CN)_{10}\subset SbF_6][SbF_6]_9$.[32] Interestingly, the two metallacyclophanes interconvert in solution in the presence of an excess of the appropriate anion.[33] These transformations are attributed to a template effect that stabilizes one particular cage over another due to favorable interactions between the anion and the central tetrazine rings.[19f,j]

Because of our ongoing interest in bptz chemistry and the desire to further investigate the role of anion$-\pi$ interactions, we have recently turned our attention to Ag(I) complexes of bptz.[28] Silver is a suitably flexible transition metal that can adopt a variety of coordination numbers and geometries,[34,35] which makes it an attractive candidate for the study of "self-healing" thermodynamic systems.[36−43] As a backdrop for the current studies, we note that the role of the anions in the assembly of Ag(I) species with terpyridine-based[44] and ethylenediamine-tetrapropionitrile[45] ligands has been investigated. In this regard, Constable et al. reported the one-dimensional (1D) polymer $\{[Ag(\mu\text{-bptz})(bptz)][BF_4]\}_\infty$, consisting of Ag(I) ions bridged by bptz ligands in the *anti* orientation and an additional chelating bptz unit binding to each ion.[46] The same group also reported the dinuclear species $[Ag_2(bptz)_2][CF_3SO_3]_2$ with bptz in the *syn* orientation.[46,47] By using the Ag(I) salt of the $[AsF_6]^-$ ion, however, we recently isolated the propeller-type compound $[Ag_2(bptz)_3][AsF_6]_2$.[28] In this structure, the anion$-\pi$ interactions that arise from the packing of the $[AsF_6]^-$ anions in the folds of the cationic propeller molecule appear to be important in the solid state.[28] To further explore similar anion$-\pi$ interactions in a systematic fashion, X-ray crystallographic as well as theoretical studies of Ag(I) complexes with the ligands bptz and the related ligand 3,6-bis(2′-pyridyl)-1,2-pyridazine (bppn; Chart 2) were undertaken. The ligand bppn was chosen for the

(14) Schneider, H. J.; Werner, F.; Blatter, T. *J. Phys. Org. Chem*. **1993**, *6*, 590.
(15) Schneider, H. J.; Blatter, T.; Palm, B.; Pfingstag, U.; Ruediger, V.; Theis, I. *J. Am. Chem. Soc*. **1992**, *114*, 7704.
(16) Schneider, H. J. *Angew. Chem*. **1991**, *103*, 1419.
(17) (a) Maeda, H.; Osuka, A.; Furuta, H. *J. Inclusion Phenom. Macrocyclic Chem*. **2004**, *49*, 33. (b) Maeda, H.; Furuta, H. *J. Porphyrins Phthalocyanines* **2004**, *8*, 67.
(18) Fairchild, R. M.; Holman, K. T. *J. Am. Chem. Soc*. **2005**, *127*, 16364.
(19) (a) Quiñonero, D.; Garau, C.; Rotger, C.; Frontera, A.; Ballester, P.; Costa, A.; Deyà, P. M. *Angew. Chem., Int. Ed.* **2002**, *41*, 3389. (b) Quiñonero, D.; Garau, C.; Frontera, A.; Ballester, P.; Costa, A.; Deyà, P. M. *Chem. Phys. Lett.* **2002**, *359*, 486. (c) Garau, C.; Frontera, A.; Quiñonero, D.; Ballester, P.; Costa, A.; Deyà, P. M. *ChemPhysChem* **2003**, *4*, 1344. (d) Garau, C.; Quiñonero, D.; Frontera, A.; Ballester, P.; Costa, A.; Deyà, P. M. *New J. Chem*. **2003**, *27*, 211. (e) Garau, C.; Frontera, A.; Quiñonero, D.; Ballester, P.; Costa, A.; Deyà, P. M. *Chem. Phys. Lett.* **2003**, *382*, 534. (f) Garau, C.; Quiñonero, D.; Frontera, A.; Costa, A.; Ballester, P.; Deyà, P. M. *Chem. Phys. Lett.* **2003**, *370*, 7. (g) Garau, C.; Frontera, A.; Quiñonero, D.; Ballester, P.; Costa, A.; Deyà, P. M. *Chem. Phys. Lett*. **2004**, *399*, 220. (h) Garau, C.; Frontera, A.; Quiñonero, D.; Ballester, P.; Costa, A.; Deyà, P. M. *J. Phys. Chem. A* **2004**, *108*, 9423. (i) Garau, C.; Frontera, A.; Quiñonero, D.; Ballester, P.; Costa, A.; Deyà, P. M. *Chem. Phys. Lett*. **2004**, *392*, 85. (j) Garau, C.; Frontera, A.; Quiñonero, D.; Ballester, P.; Costa, A.; Deyà, P. M. *Recent Res. Dev. Chem. Phys.* **2004**, 5, 227−255. (k) Quiñonero, D.; Garau, C.; Frontera, A.; Ballester, P.; Costa, A.; Deyà, P. M. *J. Phys. Chem. A* **2005**, *109*, 4632. (l) Garau, C.; Frontera, A.; Quiñonero, D.; Ballester, P.; Costa, A.; Deyà, P. M. *Eur. J. Org. Chem*. **2005**, 179. (m) Garau, C.; Quiñonero, D.; Frontera, A.; Ballester, P.; Costa, A.; Deyà, P. M. *J. Phys. Chem. A* **2005**, *109*, 9341. (n) Frontera, A.; Saczewski, F.; Gdaniec, M.; Dziemidowicz-Borys, E.; Kurland, A.; Deyà, P. M.; Quiñonero, D.; Garau, C. *Chem. Eur. J.* **2005**, *11*, 6560.
(20) Mascal, M.; Armstrong, A.; Bartberger, M. D. *J. Am. Chem. Soc.* **2002**, *124*, 6274.
(21) Yaroslav, R. S.; Lindeman, S. V.; Rosokha, S. V.; Kochi, J. K. *Angew. Chem., Int. Ed.* **2004**, *43*, 4650.
(22) Kim, D.; Tarakeshwar, P.; Kwang, S. K. *J. Phys. Chem. A* **2004**, *108*, 1250.
(23) Alkorta, I.; Rozas, I.; Elguero, J. *J. Am. Chem. Soc*. **2002**, *124*, 8593.
(24) Berryman, O. B.; Hof, F.; Hynes, M. J.; Johnson, D. W. *Chem. Commun*. **2006**, 506.
(25) Demeshko, S.; Dechert, S.; Meyer, F. *J. Am. Chem. Soc*. **2004**, *126*, 4508.
(26) Casellas, H.; Massera, C.; Gamez, P.; Manotti Lanfredi, A. M.; Reedijk, J. *Eur. J. Inorg. Chem.* **2005**, 2902.
(27) de Hoog, P.; Gamez, P.; Mutikainen, I.; Turpeinen, U.; Reedijk, J. *Angew. Chem., Int. Ed.* **2004**, *43*, 5815.
(28) Schottel, B. L.; Bacsa, J.; Dunbar, K. R. *Chem. Commun*. **2005**, 46.
(29) Crespo, O.; Canales, F.; Gimeno, M. C.; Jones, P. G.; Laguna, A. *Organometallics* **1999**, *18*, 3142.
(30) Frohn, H. F.; Giesen, M.; Welting, D.; Henkel, G. *Eur. J. Solid State Inorg. Chem*. **1996**, *33*, 841.
(31) Campos-Fernández, C. S.; Clérac, R.; Dunbar, K. R. *Angew. Chem., Int. Ed.* **1999**, *38*, 3477.
(32) Campos-Fernández, C. S.; Clérac, R.; Koomen, J. M.; Russell, D. H.; Dunbar, K. R. *J. Am. Chem. Soc.* **2001**, *123*, 773.
(33) Campos-Fernández, C. S.; Schottel, B. L.; Chifotides, H. T.; Bacsa, J.; Bera, J. K.; Koomen, J. M.; Russell, D. H.; Dunbar K. R. *J. Am. Chem. Soc.* **2005**, *127*, 12909.
(34) Khlobystov, A. N.; Blake, A. J.; Champness, N. R.; Lemenovskii, D. A.; Majouga, A. G.; Zyk, N. V.; Schröder, M. *Coord. Chem. Rev.* **2001**, *222*, 155.
(35) Cortez, S. M.; Raptis, R. G. *Coord. Chem. Rev.* **1998**, *169*, 363.
(36) Marquis, A.; Kintzinger, J.-P.; Graff, R.; Baxter, P. N. W.; Lehn, J.-M. *Angew. Chem., Int. Ed.* **2002**, *41*, 2760.
(37) Weissbuch, I.; Baxter, P. N. W.; Kuzmenko, I.; Cohen, H.; Cohen, S.; Kjaer, K.; Howes, P. B.; Als-Nielsen, J.; Lehn, J.-M.; Leiserowitz, L.; Lahav, M. *Chem. Eur. J.* **2000**, *6*, 725.
(38) Baxter, P. N. W.; Lehn, J.-M.; Baum, G.; Fenske, D. *Chem. Eur. J.* **2000**, *6*, 4510.
(39) Baxter, P. N. W.; Lehn, J.-M.; Kneisel, B. O.; Fenske, D. *Angew. Chem., Int. Ed. Engl.* **1997**, *36*, 1978.
(40) Oxtoby, N. S.; Blake, A. J.; Champness, N. R.; Wilson, C. *Proc. Natl. Acad. Sci. U.S.A.* **2002**, *99*, 4905.
(41) Baxter, P. N. W.; Lehn, J.-M.; Fischer, J.; Youinou, M.-T. *Angew. Chem., Int. Ed. Engl.* **1994**, *33*, 2284.
(42) Ruben, M.; Rojo, J.; Romero-Salguero, F. J.; Uppadine, L. H.; Lehn, J.-M. *Angew. Chem., Int. Ed.* **2004**, *43*, 3644.
(43) Withersby, M. A.; Blake, A. J.; Champness, N. R.; Cooke, P. A.; Hubberstey, P.; Li, W.-S.; Schröder, M. *Cryst. Eng*. **1999**, *2*, 123
(44) Hannon, M. J.; Painting, C. L.; Plummer, E. A.; Childs, L. J.; Alcock, N. W. *Chem. Eur. J.* **2002**, *8*, 2225.
(45) Min, K. S.; Suh, M. P. *J. Am. Chem. Soc*. **2000**, *122*, 6834.
(46) Constable, E. C.; Housecroft, C. E.; Kariuki, B. M.; Kelly, N.; Smith, C. B. *C. R. Chim.* **2002**, *5*, 425.
(47) Constable, E. C.; Housecroft, C. E.; Kariuki, B. M.; Kelly, N.; Smith, C. B. *Inorg. Chem. Commun*. **2002**, *5*, 199

Chart 2

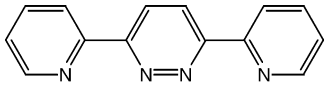

bppn

present investigation because, on the one hand, it is similar to bptz and can chelate only in the *syn* orientation,[48−50] but on the other hand, the central pyridazine ring of bppn is expected to be much less π-acidic as compared to the tetrazine ring of bptz. We note that, prior to the new studies reported herein, the triflate complexes $[Cu_4(bppn)_4][CF_3SO_3]_4$[48] and $[Ag(bppn)_2][CF_3SO_3]_2$[50] were prepared and the bis-methyl-substituted bppn species $[Ag_4(Me_2bppn)_4][CF_3SO_3]_4$ was identified by ^{1}H NMR spectroscopy to coexist with other Ag(I) mixed-ligand grids.[39] Due to the insolubility of silver halides, the Ag(I) salts of $[PF_6]^-$, $[AsF_6]^-$, $[SbF_6]^-$, and $[BF_4]^-$ were used as starting materials. To our knowledge, multiatomic anions have not been systematically explored *vis-à-vis* their role in anion−π interactions. Systems based on multiple anion−π interactions (established in our Ag(I)−bptz complexes) are promising candidates for anion-sensing receptors and transporters in biological systems.[19m]

In the work reported herein, the free ligands, as well as representative complexes, were subjected to density functional theory (DFT) calculations, and pertinent correlations were made between the derived electrostatic potentials and the solid-state structural features of the complexes. This study combines crystallographic and computational evidence that anion−π interactions are indeed present in the Ag(I) complexes with π-acidic aromatic rings and that they play an important role in determining the particular structural motif that is observed. To our knowledge, this is the first example of a comprehensive investigation of anion−π interactions as controlling elements in self-assembly reactions.

Experimental Section

A. Materials. The reagents $AgBF_4$, $AgPF_6$, $AgAsF_6$, and $AgSbF_6$ were purchased from Aldrich and used without further purification. The ligands 3,6-bis(2′-pyridyl)-1,2,4,5-tetrazine (bptz)[51] and 3,6-bis-(2′-pyridyl)-1,2-pyridizine (bppn)[52] were prepared by literature procedures and recrystallized from benzene and ethanol, respectively. All reactions were performed under an atmosphere of dry N_2 by Schlenk-line procedures. All solvents were dried by standard methods, distilled under nitrogen, and deoxygenated prior to use.

B. Physical Methods. The ^{1}H NMR spectra were recorded at 20 °C on a 500 MHz Inova spectrometer with a 5-mm switchable probehead. The ^{19}F spectra were recorded at 22 °C on a 400 MHz Unity Inova spectrometer with a 5-mm autoswitchable probe operating at 375.99 MHz. The ^{1}H NMR spectra were referenced relative to the residual proton impurities of the deuterated solvent (CD_3CN-d_3 or CD_3NO_2-d_3). The ^{19}F NMR spectra were referenced relative to $CFCl_3$ at 0 ppm. Cyclic voltammetric experiments for the free bptz and bppn ligands were carried out in CH_3CN at room temperature with 0.10 M tetra-*n*-butylammonium hexafluorophosphate as supporting electrolyte. The reduction potentials $E_{p,c}$ were referenced to the Ag/AgCl electrode without correction for junction potentials. Electrospray mass spectra were acquired on an MDS Sciex API QStar Pulsar mass spectrometer (Toronto, Ontario, Canada) using an electrospray ionization source. All spectra were acquired in positive ion mode in acetonitrile at analyte concentrations ranging between 50 and 100 μm. The spray voltage was ∼4800 V; the nozzle skimmer potential was adjusted to 10 V to minimize fragmentation.

C. Syntheses. $\{$**[Ag(bptz)][PF$_6$]**$\}_\infty$ **(1).** A fuchsia solution of bptz (50 mg, 0.21 mmol) in CH_3CN (20 mL) was added dropwise to a colorless solution of $AgPF_6$ (53 mg, 0.21 mmol) in CH_3CN (10 mL). The resulting dark purple solution was stirred for a few hours, concentrated to 7 mL, and filtered through Celite. The filtrate was layered with 20 mL of toluene. Dark violet plate-like crystals formed within 2 days. Yield: 66 mg (64%). ^{1}H NMR in CD_3CN (δ, ppm): 7.88 (ddd, J = 7.5, 5, 1 Hz, 5′,5″-H), 8.23 (ddd, J = 7.5, 1.5 Hz, 4′,4″-H), 8.88 (d, J = 7.7 Hz, 3′,3″-H), 9.05 (ddd, J = 5 Hz, 6′,6″-H). ^{19}F NMR in CD_3CN-d_3 (δ, ppm): −72.0 (d, J_{P-F} = 706 Hz, $[PF_6]^-$ free ions). ESI-MS (CH_3CN), *m*/*z*: 833 $[Ag_2(bptz)_2(PF_6)]^+$, 579 $[Ag(bptz)_2]^+$, 343 $[Ag(bptz)]^+$.

[Ag$_2$(bptz)$_2$(CH$_3$CN)$_2$][PF$_6$]$_2$ (2). A fuchsia solution of bptz (140 mg, 0.59 mmol) in CH_3CN (100 mL) was added dropwise to a colorless solution of $AgPF_6$ (150 mg, 0.59 mmol) in CH_3CN (100 mL). The resulting purple solution was stirred for 12 h, reduced in volume to ∼30 mL, layered with toluene in a thin Schlenk tube, and placed in the refrigerator. Plate-like purple crystals were collected after 3 days. Yield: 107 mg (34%). ^{1}H NMR in CD_3CN-d_3 (δ, ppm): 7.89 (ddd, J = 7.5, 5, 1.5 Hz, 5′,5″-H), 8.24 (ddd, J = 7.7 Hz, 4′,4″-H), 8.88 (d, J = 7.7 Hz, 3′,3″-H), 9.05 (ddd, J = 5 Hz, 6′,6″-H). ^{19}F NMR in CD_3CN (δ, ppm): −72.0 (d, J_{P-F} = 706 Hz, $[PF_6]^-$ free ions). ESI-MS (CH_3CN), *m*/*z*: 833 $[Ag_2(bptz)_2(PF_6)]^+$, 579 $[Ag(bptz)_2]^+$, 343 $[Ag(bptz)]^+$.

[Ag$_2$(bptz)$_2$(CH$_3$CN)$_2$][AsF$_6$]$_2$ (3). A fuchsia solution of bptz (119 mg, 0.50 mmol) in CH_3CN (85 mL) was added dropwise to a colorless solution of $AgAsF_6$ (150 mg, 0.50 mmol) in CH_3CN (100 mL) to produce a dark purple solution, which was stirred for 12 h. The solution was reduced to ∼30 mL, layered with toluene in a Schlenk tube, and placed in the refrigerator. Plate-like purple crystals were collected after 3 days. Yield: 149 mg (52%). ^{1}H NMR in CD_3CN-d_3 (δ, ppm): 7.89 (ddd, J = 6.5, 5, 1.5 Hz, 5′,5″-H), 8.24 (ddd, J = 7.9 Hz, 4′,4″-H), 8.89 (d, J = 7.9 Hz, 3′,3″-H), 9.04 (ddd, J = 5 Hz, 6′,6″-H). ^{19}F NMR in CD_3CN (δ, ppm): −65.0 (q, J_{As-F} = 932 Hz, $[AsF_6]^-$ free ions). ESI-MS (CH_3CN), *m*/*z*: 1111 $[Ag_2(bptz)_2(AsF_6)_2(CH_3CN) + H]^+$, 877 $[Ag_2(bptz)_2(AsF_6)]^+$, 579 $[Ag(bptz)_2]^+$, 343 $[Ag(bptz)]^+$.

[Ag$_2$(bptz)$_3$][AsF$_6$]$_2$ (4).[28] A fuchsia solution of bptz (178 mg, 0.75 mmol) in CH_3CN (130 mL) was added dropwise to a colorless solution of $AgAsF_6$ (150 mg, 0.50 mmol) in CH_3CN (100 mL). The resulting purple solution was stirred for 24 h, reduced to ∼30 mL, layered with toluene in a Schlenk tube, and placed in the refrigerator. Plate-like purple crystals were collected in a few days. Yield: 56.7 mg (16%). Performance of the same reaction in nitromethane induced immediate precipitation of a blue powder (evidenced by ESI-MS spectra). Yield: 276 mg (78%). ^{1}H NMR in CD_3CN-d_3 (δ, ppm): 7.87 (ddd, J = 8, 5, 1 Hz, 6H, 5′,5″-H), 8.22 (ddd, J = 7.8, 1.5 Hz, 6H, 4′,4″-H), 8.86 (d, J = 7.8 Hz, 6H, 3′,3″-H), 9.04 (ddd, J = 5 Hz, 6H, 6′,6″-H). ^{19}F NMR in CD_3CN (δ, ppm): −65.0 (q, J_{As-F} = 932 Hz, $[AsF_6]^-$ free ions). ESI-MS (CH_3CN), *m*/*z*: 923 $[Ag_2(bptz)_3 - H]^+$, 579 $[Ag(bptz)_2]^+$, 462 $[Ag_2(bptz)_3]^{2+}$, 343 $[Ag(bptz)]^+$.

[Ag$_2$(bptz)$_3$][SbF$_6$]$_2$ (5a and 5b). A fuchsia solution of bptz (92.5 mg, 0.39 mmol) in CH_3CN (130 mL) was added dropwise to a colorless solution of $AgSbF_6$ (137.5 mg, 0.40 mmol) in CH_3CN (100 mL). The resulting dark purple solution was stirred for 12 h and separated into small aliquots. Two types of crystals were grown by slow evaporation in the dark. ^{1}H NMR in CD_3CN-d_3 (δ, ppm): 7.81 (ddd, J = 7, 5, 1 Hz, 6H, 5′,5″-H), 8.20 (ddd, J = 7.7, 1.8 Hz, 6H, 4′,4″-H), 8.81 (d, J = 7.9 Hz, 6H, 3′,3″-H), 9.00 (ddd, J = 5 Hz, 6H, 6′,6″-H). ^{19}F NMR in CD_3CN (δ, ppm): −123.0 (sextet, J^{121}_{Sb-F} = 1917 Hz, octet, J^{123}_{Sb-F}

(48) Youinou, M.-T.; Rahmouni, J. F.; Fischer, J.; Osborn, J. A. *Angew. Chem., Int. Ed. Engl.* **1992**, *31*, 733.
(49) Sung, N.; Yun, K.; Kim, T.; Choi, K.; Suh, M.; Kim, J.; Suh, I.; Chin, *J. Inorg. Chem. Commun.* **2001**, *4*, 377.
(50) Constable, E. C.; Housecroft, C. E.; Kariuki, B. M.; Neuburger, M.; Smith, C. B. *Aust. J. Chem.* **2003**, *56*, 653.
(51) Geldard, J. F.; Lions, F. *J. Org. Chem.* **1965**, *30*, 318.
(52) Case, F. H. *J. Org. Chem.* **1961**, *26*, 4690.

= 1034 Hz, $[SbF_6]^-$ free ions). ESI-MS (CH_3CN), *m*/*z*: 923 $[Ag_2(bptz)_3 - H]^+$, 579 $[Ag(bptz)_2]^+$, 462 $[Ag_2(bptz)_3]^{2+}$, 343 $[Ag(bptz)]^+$.

$[Ag_4(bppn)_4][PF_6]_4$ (6). A colorless solution of bppn (138 mg, 0.59 mmol) in CH_3NO_2 (130 mL) was added dropwise to a colorless solution of $AgPF_6$ (150 mg, 0.59 mmol) in CH_3NO_2 (100 mL), resulting in a light yellow solution. The reaction solution was stirred for 12 h and then concentrated to ~30 mL. Slow diffusion of benzene into the solution for 2 days resulted in the formation of yellow block-shaped crystals. Yield: 136 mg (42%). ^{1}H NMR in CD_3NO_2-d_3 (δ, ppm): 8.73 (s, 8H, 4,5-H), 8.47 (br, d, 8H, 3′,3″-H), 8.26 (d, 8H, 6′,6″-H), 8.04 (td, 8H, 4′,4″-H), 7.48 (td, 8H, 5′,5″-H). ^{19}F NMR in CD_3NO_2 (δ, ppm): −72.2 (d, J_{P-F} = 706 Hz, $[PF_6]^-$ free ions).

$[Ag_4(bppn)_4][AsF_6]_4$ (7). A colorless solution of bppn (49 mg, 0.21 mmol) in CH_3NO_2 (130 mL) was added dropwise to a colorless solution of $AgAsF_6$ (64 mg, 0.21 mmol) in CH_3NO_2 (100 mL), resulting in the formation of a light yellow solution. After 12 h of stirring, the reaction mixture was concentrated to ~30 mL and layered with benzene. After 2 days, yellow block-shaped crystals were collected. Yield: 42 mg (33%). ^{1}H NMR in CD_3NO_2-d_3 (δ, ppm): 8.71 (s, 8H, 4,5-H), 8.46 (br, d, 8H, 3′,3″-H), 8.24 (d, 8H, 6′,6″-H), 8.03 (td, 8H, 4′,4″-H), 7.47 (ddd, 8H, 5′,5″-H). ^{19}F NMR in CD_3NO_2 (δ, ppm): −65.0 (q, J_{As-F} = 932 Hz, $[AsF_6]^-$ free ions).

$[Ag_4(bppn)_4][SbF_6]_4$ (8). A colorless solution of bppn (49 mg, 0.21 mmol) in CH_3NO_2 (130 mL) was added dropwise to a colorless solution of $AgSbF_6$ (72 mg, 0.21 mmol) in CH_3NO_2 (100 mL) to give a light yellow solution. After 12 h of stirring, the reaction mixture was concentrated to ~30 mL and layered with benzene. After 2 days, yellow block-shaped crystals were collected. Yield: 46 mg (34%). ^{1}H NMR in CD_3NO_2-d_3 (δ, ppm): 8.72 (s, 8H, 4,5-H), 8.47 (br, d, 8H, 3′,3″-H), 8.25 (d, 8H, 6′,6″-H), 8.04 (td, 8H, 4′,4″-H), 7.48 (td, 8H, 5′,5″-H). ^{19}F NMR in CD_3NO_2 (δ, ppm): −125.9 (sextet, $J_{^{121}Sb-F}$ = 1945 Hz, octet, $J_{^{123}Sb-F}$ = 1061 Hz, $[SbF_6]^-$ free ions).

$[Ag_4(bppn)_4][BF_4]_4$ (9). A colorless solution of bppn (180 mg, 0.77 mmol) in CH_3NO_2 (130 mL) was added dropwise to a colorless solution of $AgBF_4$ (150 mg, 0.77 mmol) in CH_3NO_2 (100 mL) to afford a light yellow solution. The reaction solution was stirred for 12 h, concentrated to ~30 mL, and layered with benzene, which led to the formation of yellow block-shaped crystals after 2 days. Yield: 112 mg (29.4%). ^{1}H NMR in CD_3NO_2-d_3 (δ, ppm): 8.72 (s, 8H, 4,5-H), 8.47 (br, d, 8H, 3′,3″-H), 8.26 (d, 8H, 6′,6″-H), 8.03 (td, 8H, 4′,4″-H), 7.47 (td, 8H, 5′,5″-H). ^{19}F NMR in CD_3NO_2 (δ, ppm): −153 ($[BF_4]^-$, free ions).

D. X-ray Crystallography. Single-crystal X-ray data for all compounds were collected on a Bruker APEX CCD X-ray diffractometer equipped with a graphite-monochromated Mo Kα radiation source (λ = 0.71073 Å). In a typical experiment, a crystal of appropriate size was affixed to a nylon loop with mineral oil and placed in a cold stream of N_2(g) at 110(2) K. The data were collected as three or four sets of exposures, each set having a different ϕ angle for the crystal and each exposure covering 0.3° in ω. Crystal decay was monitored by analyzing duplicate reflections and was found to be less than 1%; therefore, no decay correction was applied. The frames were integrated with the Bruker SAINT software package,[53] and a semiempirical absorption correction using multiple-measured reflections was applied using the program SADABS.[54] The structures were solved and refined using X-SEED,[55] a graphical interface to the SHELX suite of programs.[56] Additional crystallographic calculations were performed with PLATON.[57] In the final cycles of refinement, all atoms except hydrogen and disordered atoms were refined anisotropically. Aromatic hydrogen atoms were placed in geometrically optimized positions, and the bond distances and angles were idealized during refinement with the hydrogen *U* values set at 1.2 times the equivalent isotropic *U* of the C atoms to which they are attached. Methyl group hydrogen atoms were placed in regions of maximum electron density, and the bond distances and angles were idealized during refinement with the hydrogen *U* values set at 1.5 times the equivalent isotropic *U* of the C atoms to which they were attached. The crystal parameters and information pertaining to the data collection and refinement of the crystals for **1**−**9** are summarized in Table 1. Selected bond distances and angles are provided in the corresponding figure caption of each structure.

{$[Ag(bptz)][PF_6]$}$_\infty$ (1). An indexing of the preliminary diffraction patterns established that the crystal belonged to the triclinic system. The structure was solved and refined in the space group $P\bar{1}$. The asymmetric unit contains one-half each of a bptz molecule, a silver atom, and a hexafluorophosphate counterion. The final refinement cycle resulted in an *R* value of 0.0641.

$[Ag_2(bptz)_2(CH_3CN)_2][PF_6]_2$ (2) and $[Ag_2(bptz)_2(CH_3CN)_2][AsF_6]_2$ (3). An indexing of the preliminary diffraction patterns established that the crystals were monoclinic with a primitive unit cell. The structures were solved and refined in the space group $P2_1/c$. The asymmetric unit of each compound contains one bptz molecule, one silver atom, one acetonitrile ligand, and a disordered counterion ($[PF_6]^-$ and $[AsF_6]^-$ for **2** and **3**, respectively). In each case, the disorder of the anion was modeled in two different orientations; the total occupancy of both orientations was fixed to one. The final refinement cycle resulted in *R* values of 0.0776 and 0.0512 for **2** and **3**, respectively.

$[Ag_2(bptz)_3][AsF_6]_2 \cdot 2CH_3CN$ ($4 \cdot 2CH_3CN$).[28] An indexing of the preliminary diffraction patterns established that the crystal was monoclinic with a primitive unit cell. The structure was solved and refined in the space group $P2_1/c$. The asymmetric unit contains a complete $[Ag_2(bptz)_3]^{2+}$ unit, two $[AsF_6]^-$ counterions, and two acetonitrile molecules of crystallization. One of the $[AsF_6]^-$ anions was found to be disordered and was modeled in two different orientations. The final refinement cycle resulted in an *R* value of 0.0349.

$[Ag_2(bptz)_3][SbF_6]_2 \cdot 2CH_3CN$ ($5a \cdot 2CH_3CN$). Routine indexing of the diffraction patterns using the SMART[58] indexing software failed to give a reasonable unit cell. Twin indexing using the program GEMINI[59] gave a primitive orthorhombic cell with reasonable dimensions and indicated that the diffraction patterns consisted of two major components arising from a twinned or split crystal. The reflections from these components were approximately equal to each other. Precise unit-cell parameters and the correct Bravais cell were subsequently obtained using the SMART software.[58] The reflection data were integrated using the orientation matrix for only one component, with the spot size and orientation matrix for the crystal being fixed during the integration process. Some reflections overlapped, resulting in a relatively large *R* index (0.16) for merged equivalent reflections. The structure was solved and refined in the space group *Pbcn* (No. 60). The asymmetric unit contains one half of a $[Ag_2(bptz)_3]^{2+}$ molecule, one $[SbF_6]^-$ counterion, and one acetonitrile molecule of crystallization. Initially, the acetonitrile solvent molecule was refined as occupying one discrete position in the asymmetric unit, but the *U* values for these atoms and the residual electron density indicated that this molecule was disordered. The atoms belonging to this molecule were split in two parts, and their relative positions were refined. Geometric restraints were applied such that the components of disorder exhibited chemically meaningful bond distances and angles. The total occupancy of both orientations was fixed to one with the isotropic thermal parameters of both components equal. After refinement, two acetonitrile groups were rotated and displaced from

(53) *SAINT*, Program for area detector absorption correction; Siemens Analytical X-Ray Instruments Inc.: Madison, WI, 1994−1996.
(54) Sheldrick, G. M. *SADABS*, Program for Siemens area detector absorption correction; University of Göttingen: Göttingen, Germany, 1996.
(55) (a) Barbour, L. J. *X-Seed*, Graphical interface to SHELX-97 and POV-Ray; 1999 (http://www.x-seed.net). (b) Barbour, L. J. *J. Supramol. Chem.* **2001**, *1*, 189.
(56) Sheldrick, G. M. *SHELXS-97*, A Program for Crystal Structure Solution; University of Göttingen: Göttingen, Germany, 1997. Sheldrick, G. M. *SHELXL-97*, A Program for Crystal Structure Refinement; University of Göttingen: Göttingen, Germany, 1997.
(57) (a) Spek, A. L. *PLATON*; University of Utrecht: Utrecht, The Netherlands, 2001. (b) Spek, A. L. *Acta Crystallogr.* **1990**, A*46*, 194.
(58) *SMART*; Siemens Analytical X-Ray Instruments Inc.: Madison, WI, 1996.
(59) *GEMINI*, Twining solution program suite; Bruker AXS Inc.: Madison, WI, 1999.

Table 1. Crystal and Structural Refinement Data for **1**, **2**, **3**, **4**·2CH_3CN, **5a**·2CH_3CN, **5b**, **6**·4CH_3NO_2, **7**·4CH_3NO_2, **8**·4CH_3NO_2, and **9**·3CH_3NO_2·C_6H_6

	1	**2**	**3**	**4**·2CH_3CN	**5a**·2CH_3CN	**5b**	**6**·4CH_3NO_2	**7**·4CH_3NO_2	**8**·4CH_3NO_2	**9**·3CH_3NO_2·C_6H_6
formula	$AgC_{12}N_6PF_6H_8$	$Ag_2C_{28}N_{14}P_2F_{12}H_{22}$	$Ag_2C_{28}N_{14}As_2F_{12}H_{22}$	$Ag_2C_{40}N_{20}As_2F_{12}H_{30}$	$Ag_2C_{40}N_{20}Sb_2F_{12}H_{30}$	$Ag_2C_{36}N_{18}Sb_2F_{12}H_{24}$	$Ag_4C_{60}N_{20}P_4F_{24}O_8H_{52}$	$Ag_4C_{60}N_{20}As_4F_{24}O_8H_{52}$	$Ag_4C_{60}N_{20}Sb_4F_{24}O_8H_{52}$	$Ag_4C_{65}N_{19}B_4F_{16}O_6H_{55}$
formula weight	489.08	1060.28	1148.18	1384.42	1478.08	1395.97	2192.58	2368.38	2555.70	1977.00
temp (K)	110(2)	110(2)	110(2)	110(2)	110(2)	110(2)	110(2)	110(2)	110(2)	110(2)
crystal system	triclinic	monoclinic	monoclinic	monoclinic	orthorhombic	trigonal	monoclinic	monoclinic	monoclinic	monoclinic
space group	$P\bar{1}$ (No. 2)	$P2_1/c$ (No. 14)	$P2_1/c$ (No. 14)	$P2_1/c$ (No. 14)	*Pbcn* (No. 60)	$R\bar{3}$ (No. 146)	*C*2/*c* (No. 15)	*C*2/*c* (No. 15)	*C*2/*c* (No. 15)	$P2_1/c$ (No. 14)
a (Å)	7.284(2)	8.221(2)	8.288(4)	22.879(7)	25.673(9)	12.363(6)	23.316(3)	23.414(7)	23.595(5)	15.655(7)
b (Å)	7.687(2)	12.674(3)	12.736(7)	25.283(7)	8.201(3)	12.363(6)	14.237(2)	14.424(4)	14.620(3)	28.37(1)
c (Å)	7.827(2)	17.096(3)	17.504(9)	8.125(2)	23.11(2)	49.13(2)	25.069(3)	25.155(7)	25.322(5)	16.34(1)
α (°)	65.05(3)	90	90	90	90	90	90	90	90	90
β (°)	74.80(3)	97.73(3)	98.529(9)	90.353(6)	90	90	115.972(3)	116.074(4)	116.38(3)	94.79(3)
γ (°)	86.85(3)	90	90	90	90	120	90	90	90	90
V (Å^3)	382.7(2)	1765.1(6)	1827(2)	4700(2)	4865(3)	6503(5)	7481(2)	7631(4)	7826(3)	7230(7)
crystal description	needle	plate	block	plate	needle	plate	block	block	block	block
color	violet	violet	violet	violet	violet	violet	yellow	yellow	yellow	yellow
crystal size (mm^3)	0.30 × 0.20 × 0.14	0.17 × 0.13 × 0.08	0.30 × 0.21 × 0.15	0.38 × 0.26 × 0.19	0.35 × 0.18 × 0.07	0.44 × 0.24 × 0.21	0.30 × 0.25 × 0.20	0.32 × 0.19 × 0.17	0.22 × 0.13 × 0.12	0.35 × 0.10 × 0.06
Z	1	2	2	4	4	6	4	4	4	4
ρ_{calc} (g/cm^3)	2.122	1.995	2.087	1.957	2.018	2.139	1.947	2.061	2.169	1.816
μ (mm^{-1})	1.500	1.311	2.976	2.336	1.994	2.229	1.245	2.858	2.460	1.175
F(000)	238	1040	1112	2712	2856	4020	4320	4608	4896	3912
θ range (°)	2.90−27.51	2.50−27.48	1.99−27.58	0.89−27.54	2.61−26.37	1.95−27.48	1.73−27.55	2.78−27.51	2.76−28.35	1.44−26.37
diffraction limits (*h*, *k*, *l*)	$-9 < h < 8$ $-9 < k < 9$ $-10 < l < 7$	$-10 < h < 10$ $-16 < k < 15$ $-21 < l < 19$	$-10 < h < 10$ $-16 < k < 16$ $-14 < l < 22$	$-28 < h < 29$ $-32 < k < 22$ $-10 < l < 10$	$-27 < h < 13$ $-5 < k < 10$ $-28 < l < 27$	$-14 < h < 15$ $-15 < k < 16$ $-34 < l < 63$	$-30 < h < 29$ $-18 < k < 18$ $-32 < l < 31$	$-30 < h < 25$ $-18 < k < 18$ $-32 < l < 32$	$-31 < h < 31$ $-19 < k < 19$ $-32 < l < 32$	$-19 < h < 19$ $-35 < k < 35$ $-20 < l < 15$
reflections collected	2282	12888	13632	30038	12037	13296	42690	31529	33093	77086
independent reflections	1503 [*R*(int) = 0.0198]	3893 [*R*(int) = 0.0638]	4165 [*R*(int) = 0.0519]	10051 [*R*(int) = 0.0262]	4617 [*R*(int) = 0.1601]	3316 [*R*(int) = 0.0303]	8547 [*R*(int) = 0.1080]	8523 [*R*(int) = 0.0345]	9071 [*R*(int) = 0.0700]	14799 [*R*(int) = 0.0977]
completeness to θ_{max} (%)	85.6	96.0	98.1	92.5	92.7	99.6	98.8	97.1	92.7	100
data/param/restraints	1503/121/0	3893/257/30	4165/318/36	10051/687/0	4617/332/24	3316/212/0	8547/583/0	8523/587/21	9071/544/0	14799/1022/0
R,[a] w*R*[b] [$I > 2s(I)$]	0.0641, 0.1415	0.0776, 0.1897	0.0512, 0.0854	0.0349, 0.0770	0.0996, 0.1839	0.0304, 0.0715	0.0702, 0.0921	0.0362, 0.0733	0.0489, 0.1149	0.0485, 0.1124
R,[a] w*R*[b] (all data)	0.0796, 0.1480	0.1108, 0.2094	0.0748, 0.0922	0.0449, 0.0806	0.2145, 0.2281	0.0366, 0.0743	0.1231, 0.1038	0.0492, 0.0779	0.0609, 0.1211	0.1308, 0.1582
goodness-of-fit[c] (F^2)	1.069	1.050	1.079	1.088	1.019	1.047	1.108	1.032	1.060	1.046
largest diff. peak, hole (e Å^{-3})	1.653, −1.060	2.213, −1.212	0.829, −0.774	0.729, −0.533	1.401, −0.779	1.628, −1.014	0.898, −0.833	0.961, −0.613	1.535, −1.080	0.838, −0.803

[a] $R = \sum||F_o| - |F_c||/\sum|F_o|$. [b] $wR = \{\sum[w(F_o^2 - F_c^2)^2]/\sum w(F_o^2)^2]\}^{1/2}$. [c] Goodness-of-fit = $\{\sum[w(F_o^2 - F_c^2)^2]/(n - p)\}^{1/2}$, where *n* is the number of reflections and *p* is the total number of parameters refined.

each other, and the program PLATON[57] confirmed that there were no further voids accessible to solvent in the unit cell. This approach yielded a better electron density model than the refinement including one position for the acetonitrile molecule with anisotropic ellipsoids. The final refinement cycle resulted in an *R* value of 0.0996.

$[Ag_2(bptz)_3][SbF_6]_2$ (5b). Large, purple, hexagonal-shaped plates of $[Ag_2(bptz)_3][SbF_6]_2$ (**5b**) suitable for X-ray analysis grew on the sides of the container along with **5a**. Upon examination of these crystals under crossed-polarizers of an optical microscope, it was determined that they were uniaxial and had at least trigonal symmetry because they did not extinguish polarized light when viewed along their six-fold symmetry axis. The diffraction patterns had trigonal (3) Laue symmetry and were indexed in a rhombohedral unit cell that was much larger than the unit cells determined for **4** and **5a**. The structure was solved and refined in the space group $R\bar{3}$ (No. 148). The asymmetric unit contains one third of a $[Ag_2(bptz)_3]^{2+}$ molecule and two thirds of an $[SbF_6]^-$ counterion. Unlike the previous compounds, there are no solvent molecules of crystallization, and the program PLATON[57] showed that there are no solvent-accessible voids in the unit cell. The calculated density for this crystal is 2.139 g cm^{-3}, as compared to 2.018 g cm^{-3} for compound **5a**. The final refinement cycle resulted in an *R* value of 0.0304.

$[Ag_4(bppn)_4][PF_6]_4\cdot 4CH_3NO_2$ ($6\cdot 4CH_3NO_2$), $[Ag_4(bppn)_4][AsF_6]_4\cdot 4CH_3NO_2$ ($7\cdot 4CH_3NO_2$), and $[Ag_4(bppn)_4][SbF_6]_4\cdot 4CH_3NO_2$ ($8\cdot 4CH_3NO_2$). An indexing of the preliminary diffraction patterns in each case established that the crystals belonged to a monoclinic C-centered unit cell. All the structures were solved and refined in the space group *C*2/*c*. The asymmetric unit of each compound contains two bppn molecules, three silver atoms (one on a special position), two counterions ($[PF_6]^-$, $[AsF_6]^-$, and $[SbF_6]^-$ for **6**, **7**, and **8**, respectively), and two nitromethane molecules. In compounds **6** and **7**, one of the anions was found to be disordered and was modeled in two different orientations. The final refinement cycle resulted in *R* values of 0.0702, 0.0362, and 0.0489 for **6**, **7**, and **8**, respectively.

$[Ag_4(bppn)_4][BF_4]_4\cdot 3CH_3NO_2\cdot C_6H_6$ ($9\cdot 3CH_3NO_2\cdot C_6H_6$). An indexing of the preliminary diffraction patterns of **9** established that the crystals belonged to a monoclinic primitive unit cell. The structure was solved and refined in the space group $P2_1/c$. The asymmetric unit contains four bppn molecules, four silver atoms (one on a special position), four $[BF_4]^-$ counterions, one benzene, and three nitromethane molecules. One of the $[BF_4]^-$ anions was found to be disordered and was modeled in two different orientations. The final refinement resulted in an *R* value of 0.0485.

E. Theoretical Calculations. Density functional theory (DFT)[60] calculations were undertaken for the ligands bppn and bptz as well as the complexes **3**, **4**, **5b**, and **7**. The bptz and bppn ligands were subjected to full geometry optimizations in the *syn* and *anti* conformations with a triple-ζ quality basis set that had a diffuse function on the heavy atoms and a polarization function on all the atoms (6-311+G(d,p))[61] at the B3LYP [Becke three-parameter exchange functional (B3)[62] and the Lee−Yang−Parr correlation functional (LYP)[63]] level of theory as implemented in Gaussian 03 (G03).[64] Full geometry optimizations were also performed with scalar relativistic effects by the zeroth-order regular approximation (ZORA)[65] and an all-electron triple-ζ basis set with a polarization function on all atoms (TZP) designed to be used with ZORA at the BP86 [Becke exchange functional (B)[66] and Perdew−Wang correlation functional (P86)[67]] level of theory as implemented in the Amsterdam Density Functional (ADF) program.[68] Single-point energy (SPE) calculations for the crystal structure geometries were undertaken for complexes **3**, **4**, **5b**, and **7**, with scalar relativistic effects by ZORA[65] and an all-electron triple-ζ basis set with a polarization function on all atoms (TZP) designed to be used with ZORA at the BP86 level of theory,[66,67] as implemented in ADF.[68]

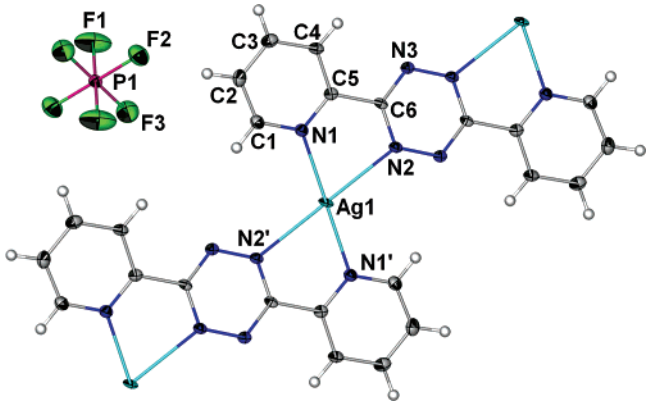

Figure 1. Thermal ellipsoid plot of a fragment of $\{[Ag(bptz)][PF_6]\}_\infty$ (**1**) at the 50% probability level. Selected bond distances (Å) and angles (°): Ag1−N1 2.218(5), Ag1−N2 2.564(5), N2−Ag1−N1 69.9(2), N1−Ag1−N1′ 180.0(2), N2−Ag1−N1′ 110.1(2), N2−Ag1−N2′ 180.0(2).

Results

A. X-ray Crystallography. $\{[Ag(bptz)][PF_6]\}_\infty$ (1). The thermal ellipsoid plot of compound **1**, a 1D coordination polymer, is depicted in Figure 1. Each Ag(I) ion resides on an inversion center and is coordinated to two bptz ligands, resulting in a distorted square planar geometry around the metal atom. The two Ag−N bond distances are Ag1−N1 2.218(5) Å and Ag1−N2 2.564(5) Å. The bptz ligands are in an *anti* orientation, which leads to the formation of the polymer. The four Ag−N bonds are coplanar, and the "bite" angles of bptz result in N−Ag−N bond angles that deviate considerably from the ideal square-planar coordination geometry (69.9(2) and 110.1(2)°). The 1D chains interact through $\pi-\pi$ contacts between the pyridyl rings (3.46 Å between π-planes) and are separated by $[PF_6]^-$ anions, which are positioned over the tetrazine rings (Figures 2a and S1). Each anion interacts with two tetrazine rings, and each tetrazine ring interacts with two different $[PF_6]^-$ anions (Figure 2a). Each anion$-\pi$ interaction involves three F atoms oriented toward the tetrazine ring (Figure 2b), with the F···tetrazine ring plane distances in the range 2.785−2.968 Å (the shortest F···tetrazine centroid distance is 2.840(5) Å).

$[Ag_2(bptz)_2(CH_3CN)_2][PF_6]_2$ (2) and $[Ag_2(bptz)_2(CH_3CN)_2][AsF_6]_2$ (3). The thermal ellipsoid plots of compounds **2** and **3**, which are isostructural, are depicted in Figures 3 and S2, respectively. In these structures, each bptz molecule is bischelating to two Ag(I) ions and is in the *syn* orientation, resulting in the formation of dinuclear cations $[Ag_2(bptz)_2(CH_3CN)_2]^{2+}$ (the Ag···Ag separations are 4.660 and 4.644 Å for **2** and **3**, respectively). Each Ag(I) ion is in a square-pyramidal geometry;

(60) Parr, R. G.; Yang, W. *Density Functional Theory of Atoms and Molecules*; Oxford University Press: New York, 1989.
(61) (a) McLean, A. D.; Chandler, G. S. *J. Chem. Phys.* **1980**, *72*, 5639. (b) Krishnan, R.; Binkley, J. S.; Seeger, R.; Pople, J. A. *J. Chem. Phys.* **1980**, *72*, 650.
(62) Becke, A. D. *J. Chem. Phys.* **1993**, *98*, 5648.
(63) Lee, C.; Yang, W.; Parr, R. G. *Phys. Rev. B* **1988**, *37*, 785.
(64) Frisch, M. J.; et al. *Gaussian 98*, Revision A.11; *Gaussian 03*, Revision B.05; Gaussian, Inc.: Pittsburgh, PA, 2003.
(65) (a) van Lenthe, E.; Baerends, E. J.; Snijders, J. G. *J. Chem. Phys.* **1993**, *99*, 4597. (b) van Lenthe, E.; Baerends, E. J.; Snijders, J. G . *J. Chem. Phys.* **1994**, *101*, 9783. (c) van Lenthe, E.; Ehlers, A. E.; Baerends, E. J. *J. Chem. Phys.* **1999**, *110*, 8943.
(66) Becke, A. D. *Phys. Rev. A* **1988**, *38*, 3098.
(67) Perdew, J. P.; Wang, Y. *Phys. Rev. B* **1986**, *33*, 8822.
(68) (a) Baerends, E. J.; et al. *ADF2004.01*; Scientific Computing and Modeling (SCM), Theoretical Chemistry, Vrije Universiteit: Amsterdam, The Netherlands, 2004 (http://www.scm.com/). (b) te Velde, G.; Bickelhaupt, F. M.; van Gisbergen, S. J. A.; Fonseca Guerra, C.; Baerends, E. J.; Snijders, J. G.; Ziegler, T. *J. Comput. Chem.* **2001**, *22*, 931. (c) Fonseca Guerra, C.; Snijders, J. G.; te Velde, G.; Baerends, E. J. *Theor. Chem. Acc.* **1998**, *99*, 391.

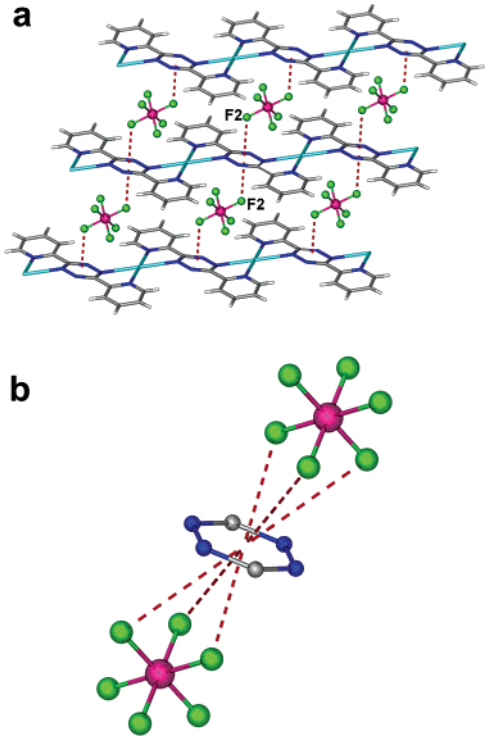

Figure 2. (a) Packing diagram of $\{[Ag(bptz)][PF_6]\}_\infty$ (**1**) depicting the shortest contacts between the $[PF_6]^-$ anions and the tetrazine ring centroids. The shortest F2···centroid distance is 2.840(5) Å; the F···tetrazine plane distances are in the range 2.785−2.968 Å. (b) Tetrazine ring with two $[PF_6]^-$ anions in **1**, displaying the three F atoms involved in each anion−π interaction (dotted lines drawn to the ring centroid).

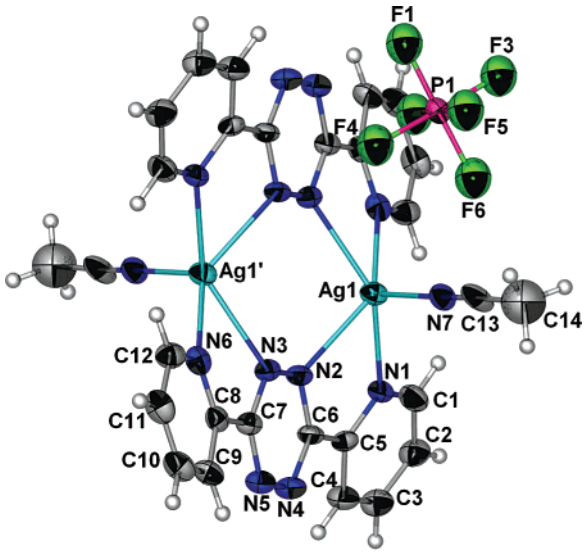

Figure 3. Thermal ellipsoid plot of $[Ag_2(bptz)_2(CH_3CN)_2][PF_6]_2$ (**2**) at the 50% probability level (one $[PF_6]^-$ ion has been omitted for clarity). The methyl carbon atom ellipsoids (C14) are depicted at the 25% probability level for the sake of clarity. Selected bond distances (Å) and angles (°): Ag1−N1 2.376(6), Ag1−N2 2.517(6), Ag1−N7 2.256(6), Ag1′-N6 2.342-(6), Ag1−N3 2.580(6), N1−Ag1−N2 68.3(2), N7−Ag1−N1 108.3(2), N7−Ag1−N2 94.7(2), N6−Ag1′−N3 67.0(3).

the fifth coordination site of the metal is occupied by an acetonitrile molecule with the two solvent molecules positioned on opposite sides of the dinuclear unit. The bptz pyridyl rings participate in intermolecular $\pi-\pi$ interactions (3.56 and 3.52 Å for **2** and **3**, respectively; Figures 4 and S3), whereas each tetrazine ring is involved in two anion−π interactions. Each

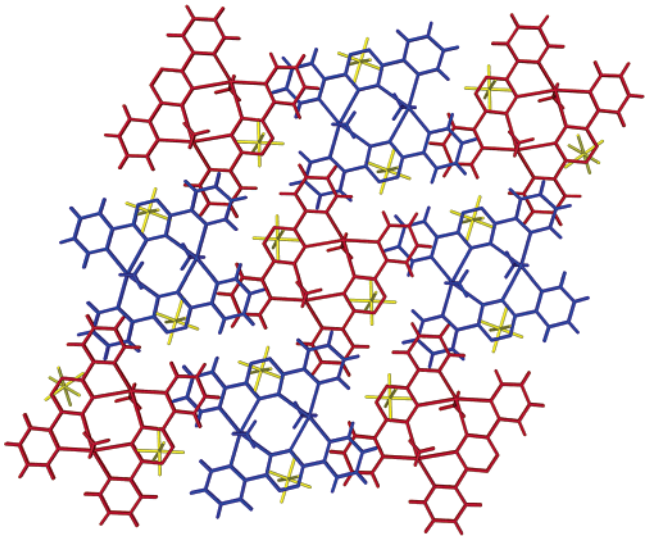

Figure 4. Packing diagram of $[Ag_2(bptz)_2(CH_3CN)_2][PF_6]_2$ (**2**) parallel to the *bc* plane.

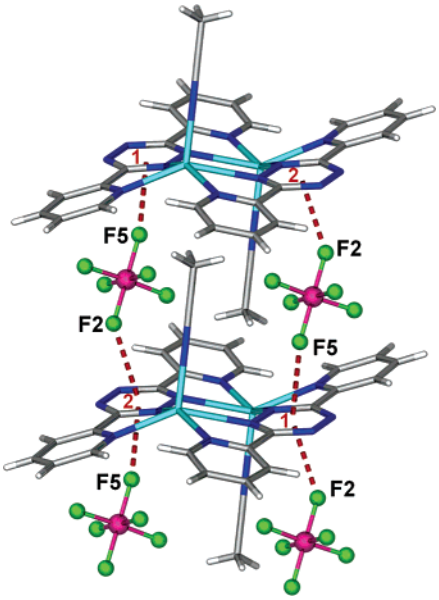

Figure 5. Portion of the crystal structure of $[Ag_2(bptz)_2(CH_3CN)_2][PF_6]_2$ (**2**) depicting the cation/anion arrangement and the shortest contacts between the $[PF_6]^-$ anions and the tetrazine ring centroids. Shortest F···tetrazine centroid distances (Å): centroid 1−F2 2.806(7), centroid 2−F5 2.835(7). The F···tetrazine plane distances are in the range 2.791−3.045 Å.

anion is sandwiched between two tetrazine rings. The anion−π interactions in **2** and **3** are depicted in Figures 5 and S4, respectively. As in the structure of **1** (Figure 2b), each anion interacts with each tetrazine ring through three F atoms oriented toward the ring, with the F···tetrazine ring plane distances in the ranges 2.791−3.045 and 2.758−3.142 Å for **2** and **3**, respectively. The shortest F···tetrazine centroid distances are 2.806(7) and 2.784(6) Å for **2** and **3**, respectively.

$[Ag_2(bptz)_3][AsF_6]_2\cdot 2CH_3CN$ (4·2CH$_3$CN) and $[Ag_2(bptz)_3][SbF_6]_2\cdot 2CH_3CN$ (5a·2CH$_3$CN). Compounds **4** and **5a** are isomorphous; the thermal ellipsoid plots of the dinuclear cations $[Ag_2(bptz)_3]^{2+}$ in **4** and **5a** are illustrated in Figures S5 and 6, respectively. In both cases, the cation consists of two Ag(I) ions (Ag···Ag separations are 4.283 and 4.320 Å for **4** and **5a**, respectively), each coordinated to six nitrogen atoms from three bptz moieties in a trigonal prismatic arrangement

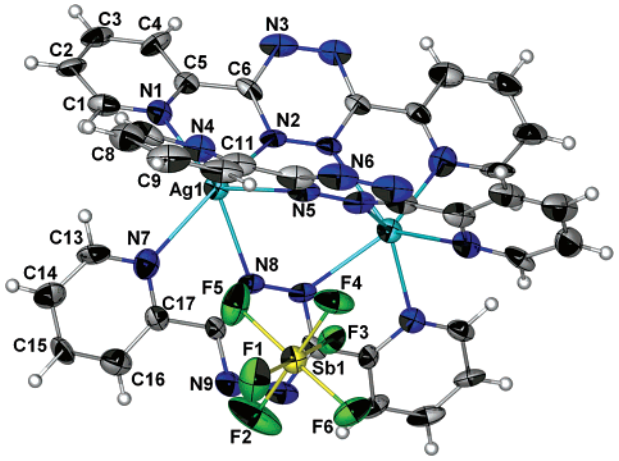

Figure 6. Thermal ellipsoid plot of $[Ag_2(bptz)_3][SbF_6]_2$ (**5a**) at the 50% probability level (one $[SbF_6]^-$ ion has been omitted for clarity). Selected bond distances (Å) and angles (°): Ag1−N1 2.451(9), Ag1−N2 2.487(9), Ag1−N4 2.491(9), Ag1−N5 2.509(8), Ag1−N7 2.41(1), Ag1−N8 2.543(9), N1−Ag1−N2 68.9(3), N2−Ag1−N8 88.5(3), N7−Ag1−N8 66.5(3), N5−Ag1−N7 118.1(3), N4−Ag1−N7 95.2(3), N1−Ag1−N4 93.7(3), N4−Ag1−N5 66.3(3).

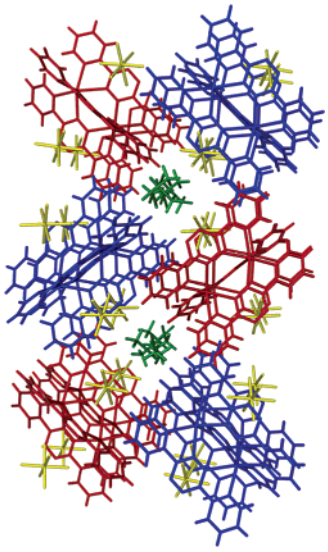

Figure 7. Packing diagram of $[Ag_2(bptz)_3][SbF_6]_2$ (**5a**) depicting the $\pi-\pi$ intermolecular interactions between pyridyl rings of bptz ligands from different propeller-type units.

with approximate C_{3v} molecular symmetry. Each bptz moiety is in the *syn* conformation and bridges the two Ag(I) ions in a bis-chelating fashion. There are $\pi-\pi$ intermolecular interactions between pyridyl rings of bptz ligands from different propeller-type units (3.52 Å for **4** and 3.51 Å for **5a**; Figures S6 and 7, respectively). Each anion ($[AsF_6]^-$ and $[SbF_6]^-$ for **4** and **5a**, respectively) interacts with two tetrazine rings from one cationic unit $[Ag_2(bptz)_3]^{2+}$ and one tetrazine ring from another cationic unit (Figures S7 and 8a**)**. Each anion interacts with each tetrazine ring through three F atoms oriented toward the ring (Figure 8b), with the F···tetrazine ring plane distances in the ranges 2.783−3.116 and 2.743−3.004 Å for **4** and **5a**, respectively **(**the shortest F···tetrazine centroid distances are 2.941(3) Å for **4** and 2.913(6) Å for **5a**). The packing of the cations and anions results in the formation of channels along the *c* axis, which are occupied by CH_3CN solvent molecules.

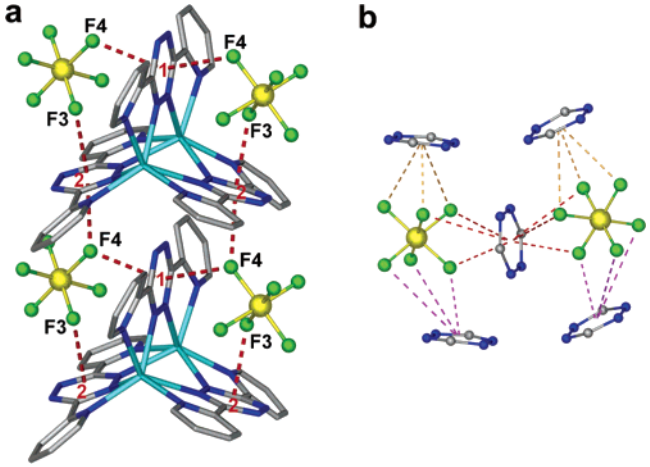

Figure 8. (a) Portion of the packing diagram of $[Ag_2(bptz)_3][SbF_6]_2$ (**5a**) depicting the cation/anion arrangement and the shortest contacts between the $[SbF_6]^-$ anions and the tetrazine ring centroids. Shortest F···tetrazine centroid distances (Å): centroid 1−F4 2.927(9), centroid 2−F4 2.913(6), centroids 2 and 3−F3 2.952(6). The F···tetrazine plane distances are in the range 2.743−3.004 Å. (b) Tetrazine ring with two $[SbF_6]^-$ anions in **5a**, displaying the three F atoms involved in each anion−π interaction (dotted lines drawn to the ring centroid).

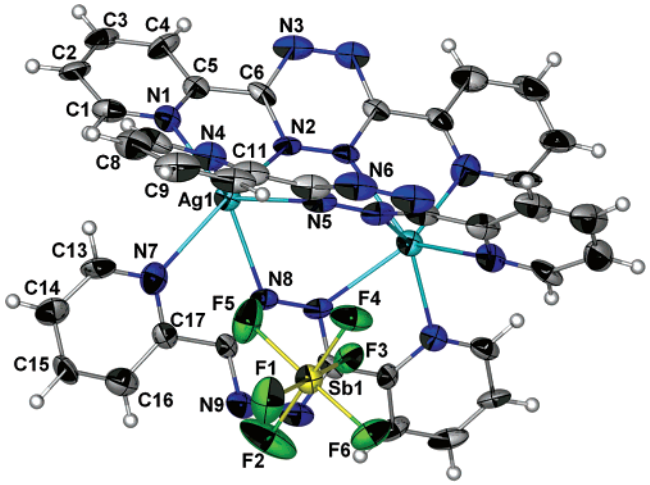

Figure 9. Thermal ellipsoid plot of $[Ag_2(bptz)_3][SbF_6]_2$ (**5b**) at the 50% probability level (one $[SbF_6]^-$ ion has been omitted for clarity). Selected bond distances (Å) and angles (°): Ag1−N1 2.438(3), Ag1−N2 2.554(3), Ag2−N3 2.575(3), Ag2−N6 2.434(3), N1−Ag1−N2 67.41(9), N3−Ag2−N6 66.19(9).

$[Ag_2(bptz)_3][SbF_6]_2$ (5b). The thermal ellipsoid plot of compound **5b** is depicted in Figure 9. Compound **5b** crystallizes in the space group $R\bar{3}$, which is the highest symmetry space group for this series of compounds. The $[Ag_2(bptz)_3]^{2+}$ unit is located on a three-fold axis and has C_{3v} symmetry, whereas two of the $[SbF_6]^-$ anions have point symmetry $\bar{3}$ and the third one is on a C_3 axis. The Ag···Ag separation is 4.424 Å, and each Ag(I) is in an ideal trigonal prismatic coordination geometry. No solvent molecules are present in the structure (Figure 10a). Unlike the other structures, this crystal does not contain cavities but consists of alternating layers of $[Ag_2(bptz)_3]^{2+}$ and $[SbF_6]^-$ ions, which are parallel to the *ab* plane (Figure 10b). One of the crystallographically independent $[SbF_6]^-$ ions is not incorporated into the anion layers; rather it participates in multiple anion−π interactions. The topology of these interactions, however, is different from that observed in **4** and **5a**. The $[SbF_6]^-$ anion is surrounded by six tetrazine rings,

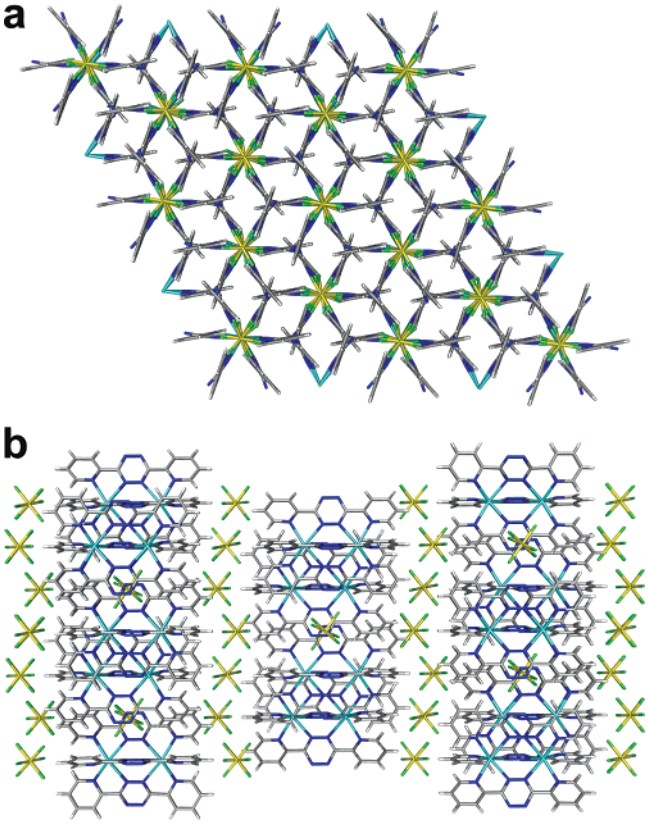

Figure 10. (a) Packing diagram of $[Ag_2(bptz)_3][SbF_6]_2$ (**5b**) along the *c* axis; (b) view perpendicular to the *c* axis.

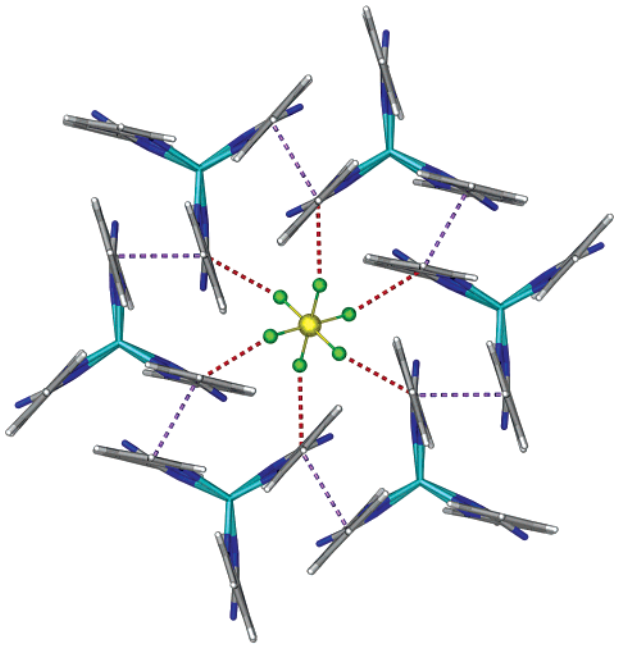

Figure 11. Anion−π interactions between a $[SbF_6]^-$ anion and six tetrazine rings in $[Ag_2(bptz)_3][SbF_6]_2$ (**5b**). The F−centroid distance is 3.265(3) Å (red dash lines); the F−tetrazine plane distance is 2.844 Å. The π−π contacts (3.36 Å) are indicated with purple dashed lines.

and each anion−π interaction involves one F atom facing the tetrazine ring plane at a crystallographically unique distance of 2.844 Å, with the shortest tetrazine centroid contact being 3.265(3) Å (Figure 11). The bptz molecules in each $[Ag_2(bptz)_3]^{2+}$ unit establish intermolecular π−π interactions with the bptz moieties of three other cationic units (Figure 11).

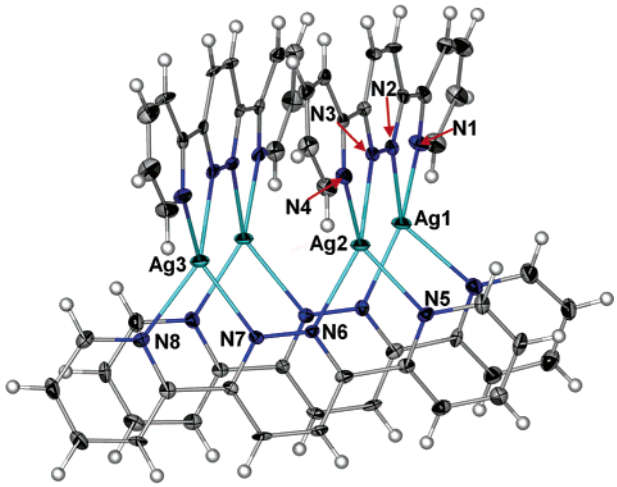

Figure 12. Thermal ellipsoid plot of the cationic unit $[Ag_4(bppn)_4]^{4+}$ in **6** at the 50% probability level. Selected bond distances (Å) and angles (°): Ag1−N1 2.319(5), Ag1−N2 2.222(4), Ag2−N3 2.369(4), Ag2−N4 2.272(4), Ag2−N5 2.288(5), Ag2−N6 2.338(4), Ag3−N7 2.284(4), Ag3−N8 2.305(4), N1−Ag1−N2 72.5(2), N3−Ag2−N4 70.7(2), N4−Ag2−N6 129.1(1), N6−Ag2−N5 71.2(2), N5−Ag2−N3 117.7(1), N7−Ag3−N8 72.2(2).

Unlike **4** and **5a**, wherein only the bptz pyridyl rings participate in π−π interactions, the π−π contacts in **5b** are maximized by involvement of both the pyridyl and tetrazine rings. The intermolecular π−π stacking between the bptz rings (3.36 Å) results in a highly symmetric crystal packing arrangement (Figures 10a and 11).

$[Ag_4(bppn)_4][PF_6]_4\cdot 4CH_3NO_2$ ($6\cdot 4CH_3NO_2$), $[Ag_4(bppn)_4][AsF_6]_4\cdot 4CH_3NO_2$ ($7\cdot 4CH_3NO_2$), and $[Ag_4(bppn)_4][SbF_6]_4\cdot 4CH_3NO_2$ ($8\cdot 4CH_3NO_2$). Compounds **6**−**8** are isostructural. The thermal ellipsoid plots of **6**, **7**, and **8** are illustrated in Figures 12, S8, and S9, respectively. Despite similar reaction conditions, compounds **6**−**8** differ considerably from the compounds obtained with bptz. In all cases, [2×2] silver grids $[Ag_4(bppn)_4]^{4+}$, similar to the cationic unit in the compound $[Cu_4(bppn)_4][CF_3SO_3]_4$,[48] are formed. The Ag(I) ions in each grid are in a distorted tetrahedral geometry, and the bppn moieties are in the *syn* orientation. The Ag···Ag separations in **6**−**8** are 3.73 Å. The Ag−N(pyridazine) and the Ag−N(pyridine) distances for **6**−**8** are in the ranges 2.220−2.370 and 2.260−2.331 Å, respectively. The grids are stabilized by intramolecular π−π interactions between both the pyridine and pyridazine rings of the bppn molecules (Figure 13a,b; 3.38, 3.38, and 3.33 Å for **6**, **7**, and **8**, respectively). No intermolecular π−π interactions are present (the packing diagram of **6** is shown in Figure S10). In **6**−**8** there is only one anion−π interaction per pyridazine ring (Figure 13a); each anion interacts with only one ring through three F atoms (Figure 13c), and the F···pyridazine ring plane distances are in the ranges 2.902−3.181, 2.780−3.092, and 2.937−3.033 Å for **6**, **7**, and **8**, respectively. The shortest F···tetrazine ring centroid distances are 3.095(6), 3.096(3), and 3.260(5) Å for **6**, **7**, and **8**, respectively.

$[Ag_4(bppn)_4][BF_4]_4\cdot 3CH_3NO_2\cdot C_6H_6$ ($9\cdot 3CH_3NO_2\cdot C_6H_6$). The thermal ellipsoid plot of **9** is illustrated in Figure 14. The structure of **9** is analogous to those of compounds **6**−**8**. Due to the lower symmetry of this structure, there are four different Ag···Ag separations in the range 3.677−3.770 Å. Each Ag(I) ion is in a distorted tetrahedral geometry, and the Ag−N-

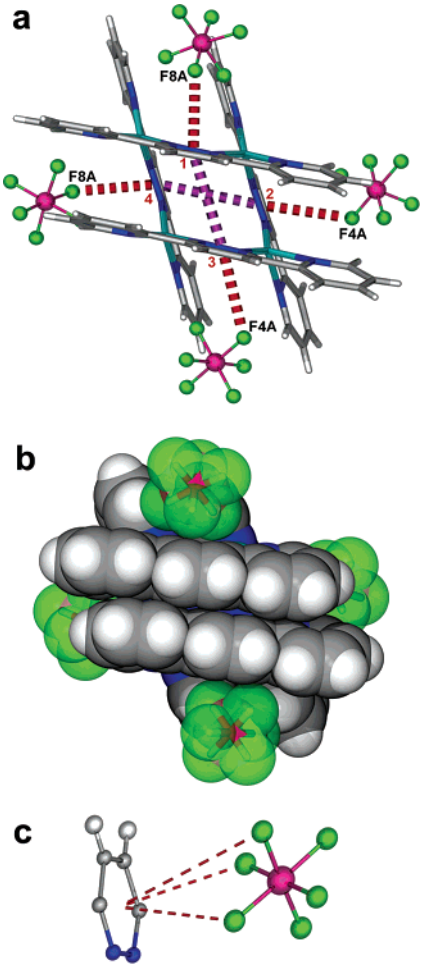

Figure 13. (a) Grid-type structure of $[Ag_4(bppn)_4][PF_6]_4$ (**6**) depicting the $\pi-\pi$ (3.38 Å; purple dashed lines) and anion$-\pi$ interactions (red dashed lines). The F···pyridazine ring plane distances are in the range 2.902−3.181 Å. Shortest F···tetrazine ring centroid distances (Å): centroids 1 and 4−F8A 3.095(6), centroids 2 and 3−F4A 3.336(4). (b) Space-filling representation of **6**. (c) Pyridazine ring with one $[PF_6]^-$ anion in **6**, displaying the three F atoms involved in each anion$-\pi$ interaction (dotted lines drawn to the ring centroid).

(pyridazine) and Ag−N(pyridine) distances are in the ranges 2.264(5)−2.360(5) and 2.279(5)−2.348(5) Å, respectively. Intramolecular $\pi-\pi$ stacking interactions at a distance of 3.53 Å between the bppn rings of the grid are present as in **6**−**8** (Figure 13a,b). In contrast to compounds **6**−**8**, however, only three out of the four pyridazine rings of the grid **9** participate in anion$-\pi$ interactions. The F···pyridazine ring plane distances are in the range 2.835−3.261 Å (the shortest F-to-tetrazine ring centroid distance is 2.897(4) Å).

B. NMR and Mass Spectrometry Studies. Ag(I)−bptz Complexes. The aromatic region of the ^{1}H NMR spectra of the Ag(I) bptz compounds **1**−**5b** in CD_3CN-d_3 exhibits four sets of resonances, which indicate that the bptz ligands are binding to the Ag(I) ions in a symmetric fashion in all cases. Complexes **1**−**5b** exhibit resonances at $\delta \approx 9.1$, 8.9, 8.2, and 7.9 ppm in CD_3CN-d_3, which are ascribed to the 6′,6″, 3′,3″, 4′,4″, and 5′,5″ protons of the pyridyl rings (Figure 15), respectively. Unbound bptz exhibits resonances at δ 8.93 (6′,6″), 8.64 (3′,3″) 8.10 (4′,4″), and 7.65 (5′,5″) ppm in CD_3CN-d_3 for the corresponding protons.[33] Thus, the 6′,6″, 3′,3″, 4′,4″, and 5′,5″ protons of the Ag(I) complex pyridyl rings shift downfield by $\Delta\delta \approx 0.2$, 0.2, 0.1, and 0.2 ppm, with respect to

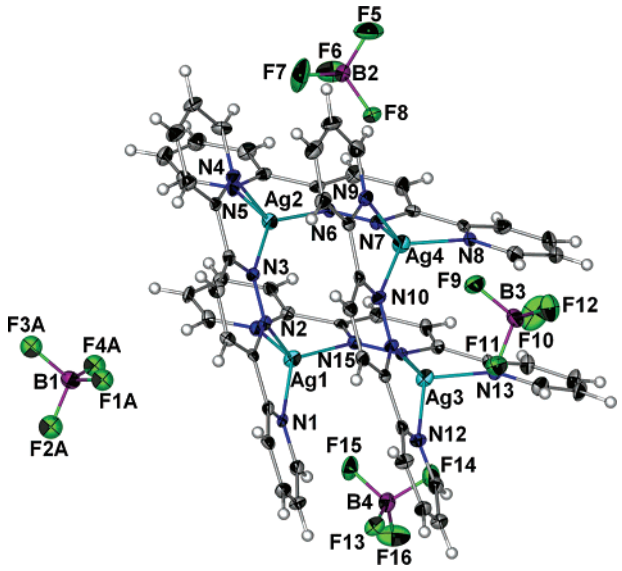

Figure 14. Thermal ellipsoid plot of $[Ag_4(bppn)_4][BF_4]_4$ (**9**) at the 50% probability level. Selected bond distances (Å) and angles (°): Ag2−N3 2.284(5), Ag2−N6 2.290(5), Ag2−N4 2.355(5), Ag2−N5 2.360(5), N3−Ag2−N4 70.9(2), N6−Ag2−N5 70.5(2), N3−Ag2−N6 138.4(2), N6−Ag2−N4 138.9(2), N3−Ag2−N5 141.0(2), N4−Ag2−N5 104.4(2).

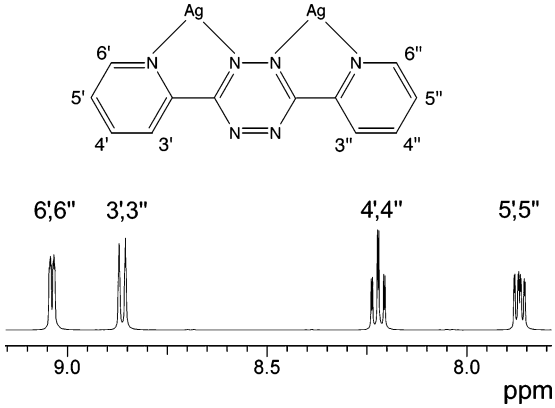

Figure 15. Aromatic region of the ^{1}H NMR spectrum of $[Ag_2(bptz)_3][AsF_6]_2$ **(4)** in CD_3CN-d_3.

the corresponding free bptz protons due to the inductive effect of the metal.[69]

The ESI-MS spectra of compounds **1**−**3** in CH_3CN exhibit peaks at *m*/*z* 579, with the appropriate isotopic distributions, that correspond to $[Ag(bptz)_2]^+$. Other disilver species observed at *m*/*z* 832 and 877 for **1**−**3** correspond to the ion clusters $[Ag_2(bptz)_2(PF_6)]^+$ and $[Ag_2(bptz)_2(AsF_6)]^+$, respectively. Compounds **1**−**3** also exhibit peaks at *m*/*z* 343, which indicate the presence of $[Ag(bptz)]^+$ ions in solution. No evidence of any higher nuclearity species in solution was obtained for the polymeric compound **1**. These observations are similar to those reported for $[Ag_2(bptz)_2][CF_3SO_3]_2$.[46,47] The ESI-MS spectra of compounds **4**−**5b** exhibit peaks at *m*/*z* 462 and 923, corresponding to $[Ag_2(bptz)_3]^{2+}$ and $[Ag_2(bptz)_3 - H]^+$, respectively (Figure S11 for **4**), which indicate the presence of the doubly and singly charged intact cationic units in solution. The presence of the $[Ag_2(bptz)_3]^{2+}$ ions under the conditions required for the mass spectral studies are indicative of the unusual stability of

(69) (a) Dijt, F. J.; Canters, G. W.; den Hartog, J. H. J.; Marcelis, A. T. M.; Reedijk, J. *J. Am. Chem. Soc.* **1984**, *106*, 3644. (b) Kong, P. C.; Theophanides, T. *Inorg. Chem.* **1974**, *13*, 1981.

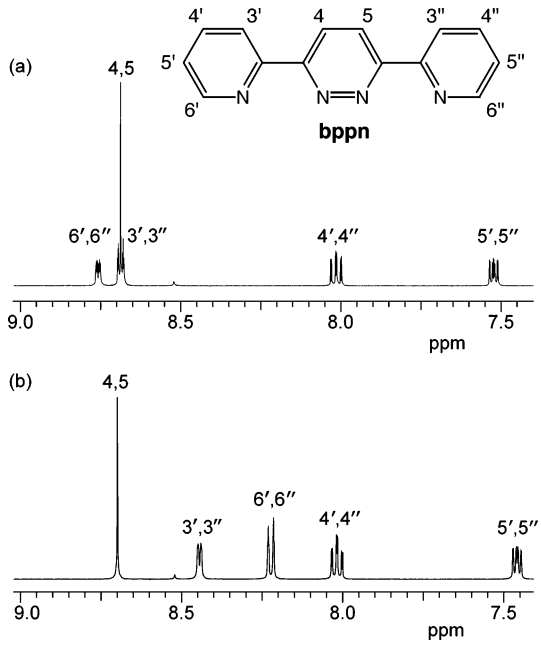

Figure 16. Aromatic region of the ^{1}H NMR spectrum of (a) bppn and (b) $[Ag_4(bppn)_4][PF_6]_4$ **(6)** in CD_3NO_2-d_3.

the Ag(I) propeller-type compounds **4**−**5b**. Compounds **4**−**5b** also exhibit peaks at *m*/*z* 579 and 343 in their ESI-MS spectra, which indicate the presence of the $[Ag(bptz)_2]^+$ and $[Ag(bptz)]^+$ ions in solution, as in the cases of compounds **1**−**3**.

In spite of the fact that compound **1** is a polymer and compounds **2**, **3** are dimers in the solid state, the shifts of their ^{1}H NMR resonances are similar, and their ESI-MS spectra indicate the presence of mononuclear and dinuclear Ag(I) species in solution.[46,47] Although the ESI-MS spectra of the propeller-type compounds **4**−**5b** support the presence of the species $[Ag_2(bptz)_3]^{2+}$, their ^{1}H NMR spectra are very similar to those of **1**−**3**. Apparently, the different Ag(I):bptz stoichiometries among compounds **1**−**5b** are not reflected by their ^{1}H NMR spectra. The downfield shifts of the protons of the Ag(I)−bptz species relative to the free ligand, albeit relatively small, indicate that there is an interaction between the Ag(I) ions and bptz units in solution,[40] but the inductive effect of the Ag(I) ions on the aromatic rings is approximately the same[70] and the ligands are binding to the Ag(I) ions in a symmetric fashion in all cases.

Ag(I)−bppn Complexes. Free bppn exhibits resonances at δ 8.77 (dd, 6′,6″-H), 8.70 (dd, 3′,3″-H), 8.70 (d, 4,5-H), 8.02 (dt, 4′,4″-H), and 7.53 (ddd, 5′,5″-H) ppm in CD_3NO_2-d_3 (Figure 16a). The aromatic region of the ^{1}H NMR spectra of the Ag(I)−bppn compounds **6**−**9** in CD_3NO_2-d_3 exhibits five sets of resonances, which indicate that the bppn ligands are binding to the Ag(I) ions in a symmetric fashion in accord with grid-like rather than oligomeric structures. Complexes **6**−**9** exhibit resonances at $\delta \approx$ 8.7, 8.46, 8.24, 8.03, and 7.47 ppm in CD_3NO_2-d_3 (Figure 16b for **6**), which are attributed to the (4,5), 3′,3″, 6′,6″, 4′,4″, and 5′,5″ protons of bppn, respectively. The resonances of the protons 3′,3″- and 6′,6″-H are shifted upfield by ~0.25 and 0.50 ppm, respectively, and have switched relative positions with respect to the free ligand resonances, features that were also observed in the ^{1}H NMR spectra of other Cu(I)−bppn and Ag(I)-functionalized bppn grid-type molecules.[48,71] The considerable upfield shift of the resonances for the proton atoms 6′,6″, adjacent to the binding sites of the Ag(I) ions, is attributed to a shielding effect from the neighboring pyridyl bppn aromatic rings of the grid.[38,72−74] Mass spectra are not reported for the Ag(I)−bppn complexes due to the unsuitability of nitromethane as a solvent for such studies (the compounds decompose in other solvents).

C. Bptz and Bppn Ligand Calculations. The ligands bptz and bppn were subjected to DFT geometry optimization calculations to determine the effect of the different number of nitrogen atoms of the central rings on the corresponding electrostatic potential. On the basis of the reduction potentials $E_{p,c}$ of the free ligands,[75] bptz is expected to be more electropositive than bppn. Both ligands were optimized in the low-energy *anti* orientation (Figures 17a,b and 18a,b), but because the ligands are *syn* in complexes **2**−**9**, they were also optimized in the higher-energy *syn* orientation (Figures 17c,d and 18c,d). The differences between the optimized geometries calculated by the B3LYP/6-311+G(d,p) and BP86/TZP optimizations are negligible for both the *syn* and *anti* orientations of bptz and bppn.

The B3LYP/6-311+G(d,p) (Figure 17) and BP86/TZP (Figure 18) optimizations afforded similar electrostatic potential maps (electrostatic potential mapped on the electron density with an isodensity value of 0.02). The electrostatic potential maps derived from B3LYP/6-311+G(d,p) and BP86/TZP calculations clearly indicate an area of positive charge, illustrated by the blue color, in the center of the bptz tetrazine ring (Figures 17a,c and 18a,c), which is more intense as compared to the bppn central pyridazine ring (Figures 17b,d and 18b,d). Moreover, for the bptz ligand, the electrostatic potential maps suggest that the central ring is significantly more electropositive as compared to the outer pyridyl rings (Figures 17a,c and 18a,c). On the contrary, the three bppn rings are very similar in charge distribution, with the central pyridazine ring being only slightly more electropositive than the outer pyridyl rings (Figures 17b,d and 18b,d).

An important observation is that, for both ligands, the electrostatic potentials do not change significantly between the low-energy *anti* and the higher-energy *syn* conformations (Figures 17 and 18). The bptz ligand displays the same increase in electropositive charge of its central tetrazine ring in both the *anti* and *syn* conformations (Figures 17a,c and 18a,c), and bppn displays a more electronegative central ring than bptz for both conformations (Figures 17b,d and 18b,d). Therefore, the charge density distributions in the Ag(I)−bptz and −bppn complexes should not be affected by the conformations of the ligands, which, except for **1**, are *syn*-oriented.

D. Silver Complex Calculations. BP86/TZP SPE calculations were undertaken for the crystal structure geometries of

(70) (a) Dijt, F. J.; Canters, G. W.; den Hartog, J. H. J.; Marcelis, A. T. M.; Reedijk, J. *J. Am. Chem. Soc.* **1984**, *106*, 3644. (b) Kong, P. C.; Theophanides, T. *Inorg. Chem.* **1974**, *13*, 1981.

(71) Hoogenboom, R.; Kickelbick, G.; Schubert, U. S. *Eur. J. Org. Chem.* **2003**, 4887.

(72) (a) Komeda, S.; Ohishi, H.; Yamane, H.; Harikawa, M.; Sakaguchi, K.; Chikuma, M. *J. Chem. Soc., Dalton Trans.* **1999**, *17*, 2959. (b) Komeda, S.; Lutz, M.; Spek, A. L.; Yamanaka, Y.; Sato, T.; Chikuma, M.; Reedijk, J. *J. Am. Chem. Soc.* **2002**, *124*, 4722.

(73) Ting, Y.; Lai, Y.-H. *J. Am. Chem. Soc.* **2004**, *126*, 909.

(74) Burgeson, J. R.; Renner, M. K.; Hardt, I.; Ferrence, G. M.; Standard, J. M.; Hitchcock, S. R. *J. Org. Chem.* **2004**, *69*, 727.

(75) Reduction potentials $E_{p,c}$ (vs Ag/AgCl) in CH_3CN: −0.81 V (bptz), −1.80 V (bppn).

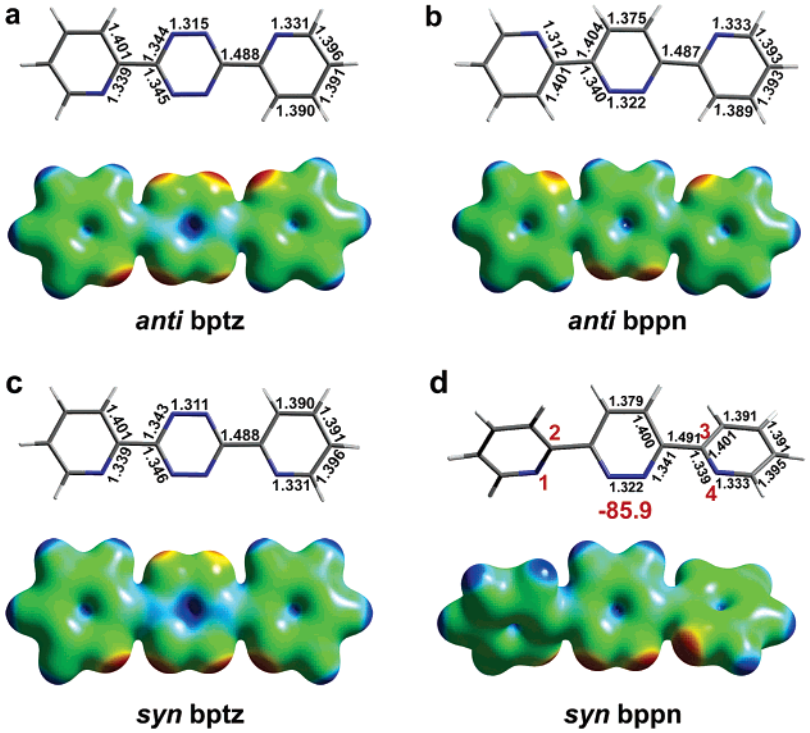

Figure 17. B3LYP/6-311+G(d,p) geometry optimization and electrostatic potential maps for (a) bptz in the *anti* orientation, (b) bppn in the *anti* orientation, (c) bptz in the *syn* orientation, and (d) bppn in the *syn* orientation (the dihedral angle defined by the atoms labeled with red numbers is −85.9°). The maps were generated with Cerius[2] 4.8 (Accelrys, Inc.) at a 0.02 isodensity value and a color scale of 126 (blue) to −63 (red) kcal/mol.

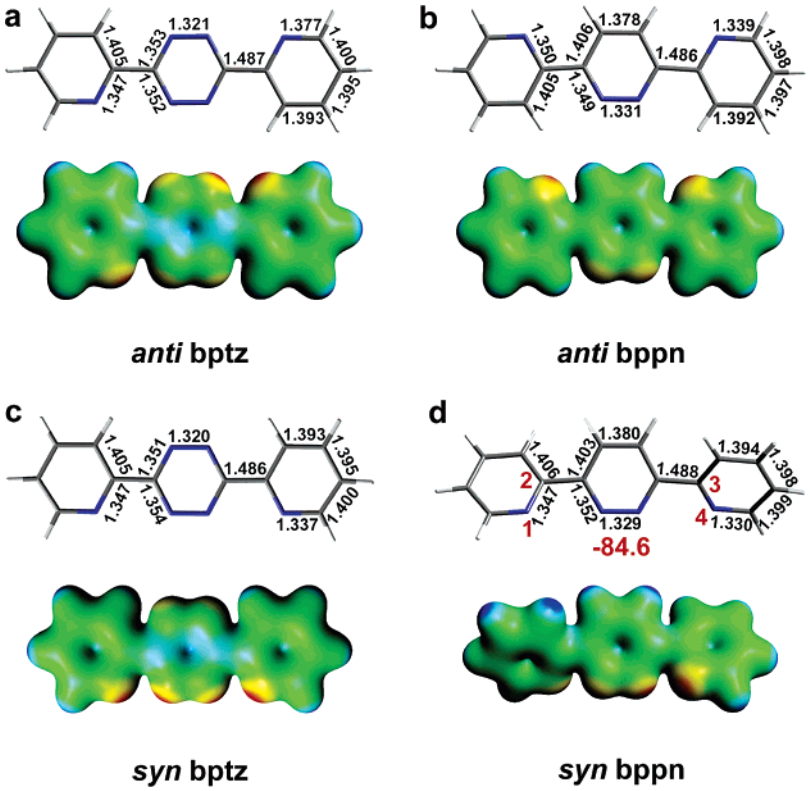

Figure 18. BP86/TZP geometry optimization and electrostatic potential maps for (a) bptz in the *anti* orientation, (b) bppn in the *anti* orientation, (c) bptz in the *syn* orientation, and (d) bppn in the *syn* orientation (the dihedral angle defined by the atoms labeled with red numbers is −84.6°). The maps were generated with the ADFView[76] interface at a 0.02 isodensity value and a color scale of 126 (blue) to −63 (red) kcal/mol.

the neutral or cationic species of **3**, **4**, **5b**, and **7**, and their electrostatic potential maps are depicted in Figures 19−23.

The electrostatic potential map scales, derived from the SPE calculations (and thus the color ranges) of the doubly charged cation $[Ag_2(bptz)_2(CH_3CN)_2]^{2+}$ (Figure 19a) and the neutral complex **3** (Figure 19b), were adjusted to have the same intensities for the outer pyridyl rings of the bptz ligands in the two differently charged species; thus, a direct comparison of

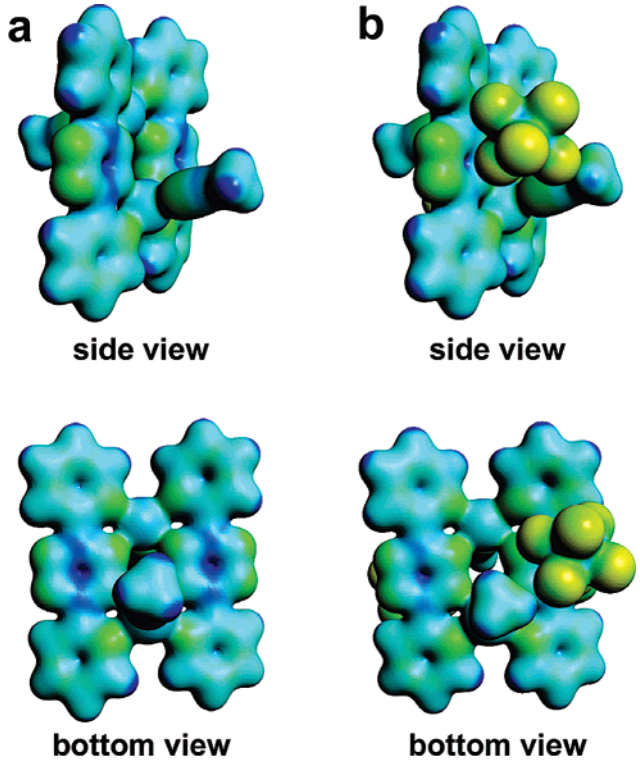

Figure 19. Electrostatic potential map from the BP86/TZP SPE calculations for **3**: (a) doubly charged cation $[Ag_2(bptz)_2(CH_3CN)_2]^{2+}$ with a color scale of 220 (blue) to −31 (red) kcal/mol, and (b) neutral complex $[Ag_2(bptz)_2(CH_3CN)_2][AsF_6]_2$ with a color scale of 126 (blue) to −126 (red) kcal/mol. The maps were generated with ADFView[76] at a 0.02 isodensity value.

colors between the electrostatic maps in Figures 19a and 19b is viable. The SPE calculations performed for **3** indicate that, in the absence of the $[AsF_6]^-$ counteranions, the cationic subunit $[Ag_2(bptz)_2(CH_3CN)_2]^{2+}$ displays a highly electropositive area in the central tetrazine ring of both bptz units as compared to the outer pyridyl rings (Figure 19a) analogous to that observed in the electrostatic maps of free bptz (Figures 17c and 18c). In the neutral complex **3**, there is equivalent charge density distribution on the two bptz ligands. The two tetrazine rings of the bptz ligands in close proximity to the $[AsF_6]^-$ anions become less electropositive as compared to the tetrazine rings in the cationic unit $[Ag_2(bptz)_2(CH_3CN)_2]^{2+}$, but the central tetrazine rings still remain more electropositive than the outer pyridyl rings (Figure 19). The decrease in the electropositive character of the central tetrazine rings in the neutral complex is attributed

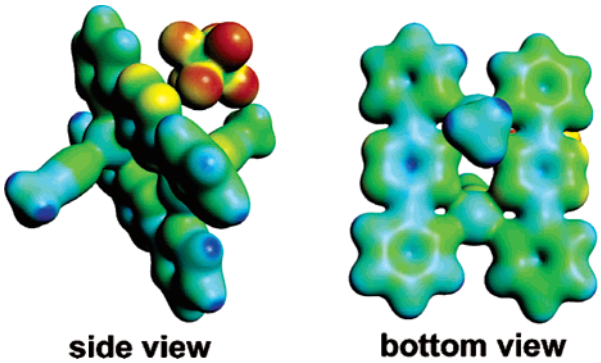

Figure 20. Electrostatic potential map from the BP86/TZP SPE calculations for the singly charged cation $\{[Ag_2(bptz)_2(CH_3CN)_2][AsF_6]\}^+$ of **3** with a color scale of 188 (blue) to −31 (red) kcal/mol. The maps were generated with ADFView[76] at a 0.02 isodensity value.

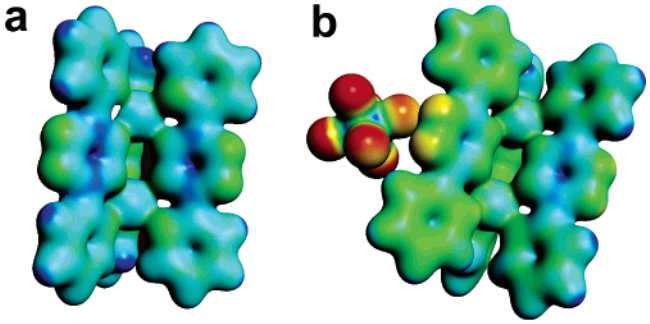

Figure 21. Electrostatic potential map from the BP86/TZP SPE calculations for **5b**: (a) doubly charged $[Ag_2(bptz)_3]^{2+}$ with a color scale of 220 (blue) to −31 (red) kcal/mol, and (b) singly charged cation $\{[Ag_2(bptz)_3][SbF_6]\}^+$ with a color scale of 188 (blue) to −31 (red) kcal/mol. The maps were generated with ADFView[76] at a 0.02 isodensity value.

to a flow of electron density from the $[AsF_6]^-$ anions to the bptz π-acidic central rings and the establishment of favorable anion−π interactions between the $[AsF_6]^-$ anions and the tetrazine rings. Although both central tetrazine rings of the neutral complex **3** are more electronegative as compared to free bptz and the dication of **3**, each tetrazine ring is electropositive enough to participate in an additional anion−π interaction, which is corroborated by the X-ray crystallographic data (*vide supra*; Figures 2b, S3, and S4).

The presence of only one $[AsF_6]^-$ anion in the singly charged species $\{[Ag_2(bptz)_2(CH_3CN)_2][AsF_6]\}^+$ of **3** disrupts the equivalent electrostatic potential distributions between the two bptz ligands (Figure 20; bottom view) as opposed to the neutral species of **3** (Figure 19b); the color range of the outer pyridyl rings in Figure 20 does not match that of the species in Figure 19, which prohibits direct comparison with them. The tetrazine ring of the bptz ligand in close proximity to the $[AsF_6]^-$ anion (right ligand in Figure 20, bottom view) has less electropositive character as compared to the other tetrazine ring of the molecule. Moreover, the anion fluorine atoms closest to the tetrazine ring are slightly less electronegative than the distal ones (Figure 20, side view), and the difference in the color intensities between the central tetrazine and the outer pyridyl rings in the bptz ligand in proximity to the anion has decreased as compared to the free ligand (Figure 20, bottom view, right ligand). The difference in the color intensities between the central tetrazine and the outer pyridyl rings in the distal bptz ligand from the anion (Figure 20, bottom view), however, is comparable to that in free bptz (Figures 17c and 18c). The aforementioned observations suggest a flow of electronic charge[19i] from the anion to the proximal bptz π-acidic central ring and the establishment of an anion−π interaction between the $[AsF_6]^-$ anion and the adjacent bptz tetrazine ring in the cationic species $\{[Ag_2(bptz)_2(CH_3CN)_2][AsF_6]\}^+$.

In the electrostatic potential maps of the doubly charged propeller-type unit $[Ag_2(bptz)_3]^{2+}$ of **5b**, there is equivalent charge density distribution on the three ligands, and the three central tetrazine rings display a more intense electropositive area as compared to the outer pyridyl rings (Figure 21a). Since in the crystal structure of **5b** only one $[SbF_6]^-$ anion is in proximity with each tetrazine ring (*vide supra*, Figure 11), the SPE calculation of the singly charged cation $\{[Ag_2(bptz)_3][SbF_6]\}^+$ was undertaken. In the electrostatic potential map of $\{[Ag_2(bptz)_3][SbF_6]\}^+$, the electropositive charge in the central tetrazine ring close to the anion has decreased as compared to

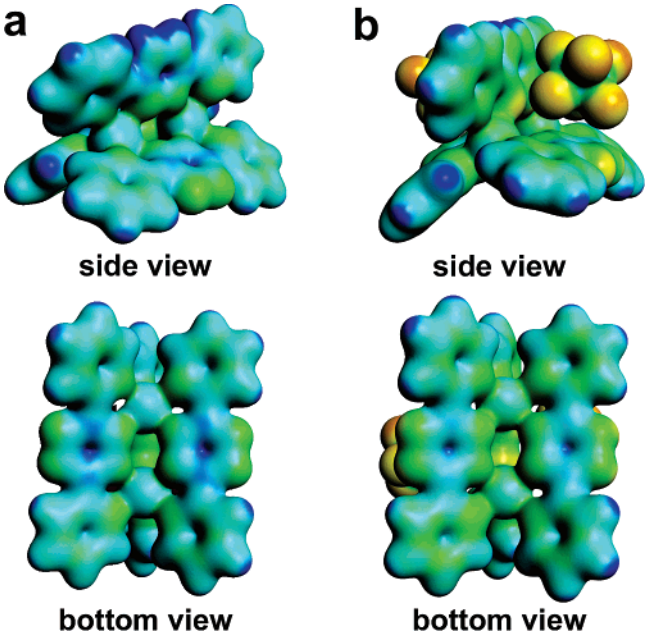

Figure 22. Electrostatic potential map from the BP86/TZP SPE calculations for **4**: (a) doubly charged cation $[Ag_2(bptz)_3]^{2+}$ with a color scale of 200 (blue) to −31 (red) kcal/mol, and (b) neutral complex $[Ag_2(bptz)_3][AsF_6]_2$ with a color scale of 126 (blue) to −94 (red) kcal/mol. The maps were generated with ADFView[76] at a 0.02 isodensity value.

the bptz ligand distal to it (Figure 21b). Furthermore, the anion fluorine atoms closest to the tetrazine ring are less electronegative than the distal ones. The previous observations suggest a flow of electronic charge[19i] from the anion to the proximal π-acidic ring and thus the presence of an anion$-\pi$ interaction between the $[SbF_6]^-$ anion and the bptz tetrazine ring.

In the electrostatic potential map of the doubly charged cationic unit $[Ag_2(bptz)_3]^{2+}$ of **4** (Figure 22a), the three tetrazine rings display a more electropositive area than the outer pyridyl rings of the bptz ligands, as observed in the free bptz ligand (Figures 17c and 18c). The higher positive charge on one of the central tetrazine rings of the dication $[Ag_2(bptz)_3]^{2+}$ (Figure 22a, upper ring, side view) originates from the bonding and geometry in the molecular crystal structure of **4** that was used for the SPE calculations. The structural features of the propeller-type compound **4** that render it less symmetric than **5b** in the solid state, account for the unequal positive charge density distribution on the three tetrazine rings of each doubly charged propeller unit $[Ag_2(bptz)_3]^{2+}$ (in contrast to equal distribution in the doubly charged species of **5b**; Figure 21a).

In contrast to the propeller-type complex **5b**, wherein only one $[SbF_6]^-$ anion is in proximity with each tetrazine ring in the crystal structure (*vide supra*: Figure 11), in **4** both $[AsF_6]^-$ anions are close to tetrazine rings (Figure S7); thus, SPE calculations of the neutral complex $[Ag_2(bptz)_3][AsF_6]_2$ were undertaken. The color scales for the dication and the neutral species in Figure 22 were adjusted to be the same for the pyridyl rings; therefore, direct color comparison between them is meaningful. In the neutral complex **4**, the positive charge density on all the central tetrazine rings has decreased (Figure 22b, bottom view) as compared to the doubly charged species (Figure 22a, bottom view), due to flow of electronic charge from the anions to the π-acidic rings in proximity to them (each anion interacts with two tetrazine rings from one cationic unit; Figure S7). These findings corroborate the presence of anion$-\pi$ interactions between the $[AsF_6]^-$ anions and the bptz tetrazine rings.[19i] The decrease in the electropositive character of the tetrazine in the upper ligand of the neutral complex (Figure 22b, side view), however, is more appreciable than in the other two tetrazine rings (Figure 22b, bottom view), despite the former being more electropositive than the latter two in the doubly charged species. This difference is attributed to two anions interacting with the upper tetrazine ring as compared to one anion per ring for the two lower rings (Figure 22b, side view). The fact that the changes in the electron density maps between the dication and the neutral species for the propeller-type complex **4** (Figure 22) follow the same trends as those in **5b**, which is a propeller-type compound with more symmetric structural characteristics (Figure 21), indicates that the anion$-\pi$ interactions claimed for **4** on the basis of the electrostatic potential maps are indeed viable.

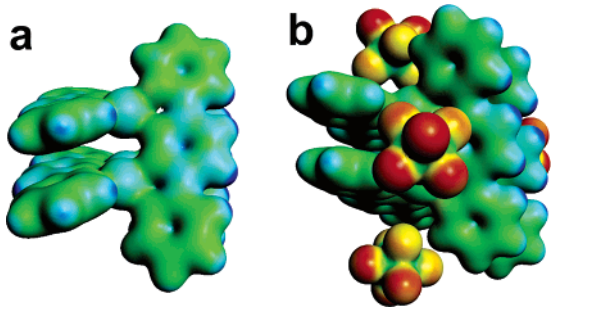

Figure 23. Electrostatic potential map from the BP86/TZP SPE calculations for **7**: (a) cationic unit $[Ag_4(bppn)_4]^{4+}$ with a color scale of 314 (blue) to −126 (red) kcal/mol, and (b) neutral complex $[Ag_4(bppn)_4][AsF_6]_4$ with a color scale of 157 (blue) to −63 (red) kcal/mol. The maps were generated with ADFView[76] at a 0.02 isodensity value.

As a representative of the bppn grid-type complexes, the cationic unit $[Ag_4(bppn)_4]^{4+}$ (Figure 23a), as well as the neutral complex $[Ag_4(bppn)_4][AsF_6]_4$ (**7**) (Figure 23b), was subjected to SPE calculations. In the cationic unit $[Ag_4(bppn)_4]^{4+}$, the slightly larger difference in the charge between the central and outer rings (Figure 23a) as compared to that of free bppn (Figures 17d and 18d) can be attributed to an induced positive charge on the central pyridazine ring due to the Ag(I) cation binding.[27] This difference in electron density between the central and outer rings of the bppn ligands in the cationic complex, however, is still much less than the difference between the tetrazine and pyridyl rings of free bptz (Figures 17c and 18c). Additionally, the change in electropositive character of the central rings of the bppn ligands in the cationic unit $[Ag_4(bppn)_4]^{4+}$ is very small upon addition of the $[AsF_6]^-$ anions (Figure 23; the color scales for the outer pyridyl rings were adjusted to be the same; therefore, direct color comparison between the cationic and neutral species is possible), which indicates the negligible flow of electron density from the anion to the pyridazine ring in the neutral complex. These results concur with a more electron-rich bppn central pyridazine ring and, thus, much weaker anion$-\pi$ interactions in **7** as compared to those established in the bptz complexes **3**, **4**, and **5b**. It is notable that for the free bppn ligand, the N−C−C−N dihedral angles are in the range −84.6 to −85.9° (Figures 17d and 18d; atoms labeled with red numbers), whereas in structures **6**−**9**, the corresponding N−C−C−N dihedral angles range from −17.7 to −22.3°. As mentioned earlier, however, the ligand conformation appears to have little effect on the electrostatic potential maps.

Discussion

Effect of Anion Identity and Anion−π Interactions on the Products. The reactions of bptz with the appropriate AgX salts (X = $[PF_6]^-$, $[AsF_6]^-$, $[SbF_6]^-$) afford complexes of three different structural types, depending on the experimental conditions and the anion used. Reactions of Ag(I) and bptz, in a 1:1 ratio, in the presence of $[PF_6]^-$ ions afford either the polymer **1** or the discrete molecular compound **2** (more concentrated solutions favor the polymer), whereas in the presence of $[AsF_6]^-$ ions, the reaction produces only the dinuclear product **3**. When the ratio of Ag(I):bptz is 2:3, the propeller-type compound $[Ag_2(bptz)_3][AsF_6]_2$ **(4)** is formed in high yield in the presence of the $[AsF_6]^-$ ions, but not in the presence of $[PF_6]^-$ ions. At a $[AgPF_6]$:bptz ratio of 2:3, only the polymer **1** or the dimer **2** is obtained in low yield (depending on the concentration of the initial solution). Reactions of Ag(I):bptz in a 1:1 ratio in the presence of $[SbF_6]^-$ ions, however, yield the propeller-type compounds **5a** and **5b**, as indicated by the single-crystal X-ray structural determinations. When the reaction is performed in a $[AgSbF_6]$:bptz ratio of 2:3, no crystals are obtained, but the propeller-type species $[Ag_2(bptz)_3]^{2+}$ is formed, as suggested by an ESI-MS spectrum of the reaction solution (ion peaks are observed at *m*/*z* 923 and 462, corresponding to the singly and doubly charged species $[Ag_2(bptz)_3 - H]^+$ and $[Ag_2(bptz)_3]^{2+}$, respectively). Attempts to react $AgBF_4$ with bptz in a 1:1 ratio lead to immediate precipitation of an insoluble product. Dissolution of the solid after prolonged heating and layering with toluene affords crystals of the previously reported compound $\{[Ag(\mu\text{-bptz})(bptz)][BF_4]\}_\infty$.[46]

Apart from the anion size (the size of the anions increases in the order $[PF_6]^- < [AsF_6]^- < [SbF_6]^-$),[76,77] which plays a role in the packing of the resulting structures, anion−π interactions appear to be a dictating factor in determining the preferred structural motif. This conclusion is corroborated by the fact that reactions of bppn with the AgX salts (X = $[PF_6]^-$, $[AsF_6]^-$, $[SbF_6]^-$, $[BF_4]^-$) in a 1:1 ratio lead only to the grid-type structures **6**−**9**, regardless of the anion present. Even when the reactions are performed with a Ag(I):bppn ratio 2:3, no propeller-type compounds are obtained with this ligand. Despite the different shapes and sizes of the various anions, all the bppn structures adopt the grid motif, which is stabilized by intramolecular π−π stacking interactions between the bppn aromatic rings.

Solid-State Evidence for Anion−π Interactions. Compound **1** is a 1D polymer, whereas compounds **2**−**5b** consist of discrete molecular units. In **1**, the bptz units are in the *anti* orientation (Figure 1), which is necessary for the formation of the polymer, whereas the bptz units in **2**−**5b** are in the *syn* orientation (Figures 3, S2, S5, 6, and 9). Bptz ligands in the *anti* orientation were also observed in the recently reported 1D polymers $\{[Ag(\mu\text{-bptz})(bptz)][BF_4]\}_\infty$[46] and $[Cd(\mu\text{-bptz})(NO_3)_2]_\infty$;[78] the metals are six-coordinate in both the latter cases, in contrast to the square planar geometry of the Ag(I) ions in **1**. Compounds **2** and **3** are 1:1 isomorphous Ag(I):bptz complexes consisting of dinuclear cationic units $[Ag_2(bptz)_2(CH_3CN)_2]^{2+}$ (Figures 3 and S2), similar to that in $[Ag_2(bptz)_2][CF_3SO_3]_2$ [46,47] with the exception that the Ag(I) ions are in a five-coordinate square pyramidal geometry instead of being square planar. The previously mentioned bptz cationic units in **2** and **3** are favored over the [2×2] grids encountered in the cations $[Ag_4(bppn)_4]^{4+}$ of the bppn compounds **6**−**9**, as well as in $[Cu_4(bppn)_4][CF_3SO_3]_4$.[48] Grid-like structures were predicted by Constable et al. to result from reactions of Ag(I) salts (X = $[BF_4]^-$, $[NO_3]^-$, or $[CF_3SO_3]^-$) with bptz, but the products are, in fact, dinuclear.[46] The formation of the dinuclear cations in **2** and **3**, instead of grids, is attributed to the favorable anion−π interactions established between the anions and the π-acidic central tetrazine rings of the bptz ligands.

In the propeller-type compounds **4**[28] and **5a**, three bptz ligands span two Ag(I) ions in the *syn* orientation (Figures S5 and 6, respectively), with the anions being situated in the folds of the cations (Figures S6 and 7, respectively); each anion establishes anion−π interactions with three tetrazine rings (Figures S7 and 8a, respectively). Likewise, in the reported two-dimensional sheet-like structure of $\{[Ag_2(dpztz)_3][SbF_6]_2\}_\infty$[40] (dpztz = 3,6-dipyrazin-2-yl-(1,2,4,5)-tetrazine), each $[SbF_6]^-$ anion interacts with three tetrazine rings at F···ring distances in the range 2.764−3.111 Å. In **5b**, the $[SbF_6]^-$ anion that is participating in the anion−π interactions is surrounded by six tetrazine rings, each F atom facing a ring at a crystallographically unique distance of 2.844 Å from the ring plane (Figure 11). To our knowledge, complex **5b** represents the first crystallographic example of an anion−π_6 system, with six anion−π interactions per participating anion. Precedent of an anion establishing anion−π interactions with four or five electron-deficient tetrazine rings was obtained from the crystal structures of the molecular Ni(II) and Zn(II) squares or the Ni(II) pentagon, respectively, with the anions encapsulated in the cavities.[31−33]

Unlike compounds **1**−**5a**, wherein only the pyridyl rings of bptz participate in π−π intermolecular stacking interactions, in **5b** all the bptz rings engage in such interactions. The structural features of compounds **5a** and **5b** render them good candidates to estimate the strength of anion−π interactions. Compound **5b** is the only bptz complex in which the central tetrazine ring of bptz participates in π−π stacking interactions. Apart from π−π stacking interactions, the central tetrazine ring of bptz in **5b** establishes anion−π interactions on the other side of the ring (Figure 11), whereas in **5a** it is participating only in anion−π interactions on both sides of the ring (Figure 8). On the basis of the fact that one cannot favor the crystallization of **5a** over **5b** and vice versa, it may be claimed that the two compounds have approximately the same overall energy, which suggests that the strength of the anion−π interactions in these compounds is comparable to that of π−π stacking (1−50 kJ/mol).[3,79] For purposes of comparison, the interaction energies obtained theoretically by Frontera et al.[19f,j] for *s*-tetrazine with Cl^- and Br^- anions and by Mascal et al.[20] for *s*-triazine with anions are less than 42 kJ/mol.

Compounds **6**−**9** form Ag(I) [2×2] square grids consisting of discrete $[Ag_4(bppn)_4]^{4+}$ cationic units (Figures 12, S8, S9, and 14), similar to those encountered in $[Cu_4(bppn)_4][CF_3SO_3]_4$,[48] instead of dinuclear or propeller-type structures. A [2×3] rectangular mixed-ligand Ag(I) grid, as well as the square [2×2] grid $[Ag_4(Me_2bppn)_4]^{4+}$, was obtained with the bis-methyl-substituted form of bppn.[39] The recently reported salt $[Ag(bppn)_2][CF_3SO_3]$ is not a grid-type compound, however,

(76) *ADFview 2004.01*; SCM, Theoretical Chemistry, Vrije Universiteit: Amsterdam, The Netherlands, 2004 (http://www.scm.com).
(77) Mingos, D. M. P.; Rohl, A. L. *Inorg. Chem.* **1991**, *30*, 3769.
(78) Du, M.; Bu, X.-H.; Biradha, K.; Shionoya, M. *J. Chem. Res.* **2002**, 247.
(79) Hunter, C. A.; Sanders, J. K. M. *J. Am. Chem. Soc.* **1990**, *112*, 5525.

Table 2. Anion−π and π−π Distances for the Central Rings in Compounds **1**−**9**

Bptz Complexes

compd	anion involved	rings per anion[a]	F distance range (Å)[c]	shortest F···centroid distance (Å)	π–π distance between tetrazine rings (Å)
1	$[PF_6]^-$	2	2.785−2.968	2.840(5)	*d*
2	$[PF_6]^-$	2	2.791−3.045	2.806(7)	*d*
3	$[AsF_6]^-$	2	2.758−3.142	2.784(6)	*d*
4	$[AsF_6]^-$	3	2.783−3.111	2.913(2)	*d*
5a	$[SbF_6]^-$	3	2.743−3.004	2.913(6)	*d*
5b	$[SbF_6]^-$	6[b]	2.844	3.265(3)	3.36

Bppn Complexes

compd	anion involved	rings per anion[e]	F distance range (Å)[g]	shortest F···centroid distance (Å)	π–π distance between pyridazine rings (Å)[h]
6	$[PF_6]^-$	1	2.902−3.181	3.095(6)	3.38
7	$[AsF_6]^-$	1	2.780−3.092	3.096(3)	3.38
8	$[SbF_6]^-$	1	2.937−3.033	3.260(5)	3.33
9	$[BF_4]^-$	1[f]	2.835−3.261	2.90(4)	3.53

[a] Number of tetrazine rings involved in anion−π interactions with each anion. [b] Only one of the two anions per molecule participates in anion−π interactions. [c] F···tetrazine plane distances. [d] No π−π interactions established. [e] Number of pyridazine rings involved in anion−π interactions with each anion. [f] Only three of the four anions per molecule participate in anion−π interactions. [g] F···pyridazine plane distances. [h] Intramolecular interactions.

and no anion−π interactions are present; instead, there is extensive π−π stacking between all the rings of the coplanar ligands within the dinuclear unit as well as between dinuclear units of the arrays.[50] Likewise, in compounds **6**−**9**, the three rings of bppn, including the central pyridazine ring, participate in intramolecular π−π stacking interactions within the grids (Figure 13a,b), with the anion−π interactions being weaker and secondary to the structure formation. In contrast, in **1**−**5b**, there are no intramolecular π−π interactions; in **1**−**5a**, intermolecular π−π stacking is established only between the bptz outer pyridyl rings. The highly π-acidic central tetrazine rings in **1**−**5a** prefer to engage in multiple anion−π interactions, instead. In compounds **1**−**5a**, each anion establishes anion−π interactions with several tetrazine rings (Table 2), and each central tetrazine ring interacts with two different anions positioned on either side of the ring (Figures 2b and 8b). Moreover, as mentioned earlier, in **5b**, one of the two $[SbF_6]^-$ anions present in the molecule participates in anion−π interactions with six tetrazine rings (Figure 11, Table 2). In compounds **6**−**8**, however, only one anion−π interaction is established per pyridazine ring (the opposite side of the pyridazine ring is involved in π−π stacking), and each anion interacts with one ring only (Figure 13a,c; in **9**, only three out of the four pyridazine rings of each grid interact with a $[BF_4]^-$ ion). The multiple anion−π interactions per anion established in the case of the bptz complexes (as compared to one per anion in the bppn complexes) and the difference in the preferred structural motifs between the bptz and bppn structures are in accord with the higher π-acidic character of the bptz central tetrazine ring as compared to the more electron-rich bppn pyridazine ring.

Favorable anion−π interactions exist between the anions and the tetrazine rings in the previously reported compounds $\{[Ag(\mu\text{-bptz})(bptz)][BF_4]\}_\infty$[46] (one per anion; F···tetrazine ring plane 2.98 Å) and $\{[Ag_2(dpztz)_3][SbF_6]_2\}_\infty$[40] (three per $[SbF_6]^-$ anion; F···tetrazine ring plane 2.7−3.1 Å), and the F···tetrazine distances are in the same range as those for the Ag(I)−bptz structures reported herein. The F···tetrazine ring (plane) distances (for the F atoms facing the rings) in the Ag(I)−bptz compounds **1**−**5b** are in the range 2.7−3.1 Å, whereas the F···pyridazine ring (plane) distances in the Ag(I)−bppn compounds **6**−**9** are in the range 2.8−3.3 Å (a nonbonded anion−π contact is considered to be present when the distance between the anion and the π-ring is less than the sum of the van der Waals radii, according to Frontera et al.[19j]). The distances of the anion F atoms facing the central ring (from the central ring plane) in the bppn compounds **6**−**9** are, in general, longer by 0.15−0.20 Å as compared to those encountered in the bptz structures **1**−**5b**, except for **7** (Table 2; the shorter distance in **7** may be attributed to the disorder of the $[AsF_6]^-$ anion, which reduces the average degree of interaction between the anion and the pyridazine ring). Since it is logically anticipated that longer anion−π distances correlate with weaker interactions of this type,[26] the 0.15−0.20 Å difference in the F···central ring distances between the bptz and bppn complexes reflects the stronger anion−π interactions involved in the bptz complexes.

The 0.15−0.20 Å difference in the F···central ring distances between the bptz and bppn complexes is comparable to that in the calculated distances between the fluorinated F_3triazine + halogen and triazine + halogen systems (and the same anion) reported by Mascal et al.;[20] the energy values of the (more π-acidic) F_3triazine systems with the shorter anion−π interactions are half the energy values of the triazine systems.[20] Furthermore, stronger anion−π interactions in the bptz as compared to bppn complexes can be argued on the basis of the multiple (between two to six) tetrazine rings participating in anion−π interactions per anion in the bptz complexes **1**−**5b**, in contrast to only one pyridazine ring interacting per anion in the bppn complexes **6**−**9** (Table 2). The additivity of anion−π interactions was recently reported by Frontera et al.;[19m] the binding energies obtained from *ab initio* studies, performed on complexes of halide ions (Cl^-, Br^-) interacting with two (or three) trifluoro-*s*-triazine (or *s*-triazine) rings, are approximately 2 (or 3) times the binding energy of the corresponding complex with only one ring interacting with the anion.[19m]

Theoretical Evidence of Anion−π Interactions. B3LYP/6-311+G(d,p) and BP86/TZP geometry optimizations and electrostatic potential calculations indicate that bptz is more likely to participate in anion−π interactions than bppn (Figures 17 and 18). In both ligands, the central rings display a more electropositive area compared to the outer pyridyl rings, but due to the four electron-withdrawing nitrogen atoms on the central ring of bptz compared to two in bppn, a significantly more electropositive area is observed in the bptz central tetrazine ring. An enhancement of the positive charge in the ring with the higher number of electronegative atoms, comparable to that between the bptz and the bppn central rings, has been observed between trifluoro-1,3,5-triazine and 1,3,5-triazine[20] as well as between C_6F_6 and benzene.[23] The relatively higher electropositive charge[19f] of the bptz central tetrazine ring (Figures 17a,c and 18a,c) suggests that bptz is likely to participate in stronger anion−π interactions as compared to bppn. This is corroborated by *ab initio* calculations on the *s*-tetrazine ring, indicating that it is a good candidate for establishing favorable anion−π interactions.[19f] On the other hand, the smaller electropositive charge of the bppn central pyridazine ring, indicated by the

charge distribution in the electrostatic potential maps (Figures 17b,d and 18b,d), suggests that it will participate in weaker anion−π interactions.

The SPE calculations for the dicationic units of the Ag(I)−bptz complexes **3** (Figure 19a), **4** (Figure 22a), and **5b** (Figure 21a) reveal the expected positive charge accumulation in the central tetrazine rings of the three bptz ligands. In their electrostatic potential maps, the difference in the color intensities between the central tetrazine and the outer pyridyl rings of the complex bptz ligands (Figures 19a, 21a, and 22a) is comparable to the difference in free bptz (Figures 17a,c and 18a,c). In the electrostatic potential map of the singly charged cationic unit $\{[Ag_2(bptz)_2(CH_3CN)_2][AsF_6]\}^+$ of **3** (Figure 20), this difference is also comparable to that in free bptz for the distal bptz ligands from the anion. In the electrostatic potential maps of the neutral bptz complexes **3** and **4** (Figures 19b and 22b), and in the singly charged cationic units of **3** (Figure 20, bottom view) and **5b** (Figure 21b), however, the difference in the color intensities between the central tetrazine and the outer pyridyl rings in the bptz ligands in proximity to the anions decreases considerably compared to that of the free ligand (Figures 17a,c and 18a,c). In the same vein, when the electrostatic map colors are adjusted properly, the F atoms closest to the tetrazine ring are less electronegative than the distal ones to the bptz moieties (Figures 20, side view, and 21b). Additionally, in the electrostatic potential maps of the neutral bptz complexes **3** and **4** (Figures 19b and 22b), and in the singly charged cationic units of **3** (Figure 20, bottom view) and **5b** (Figure 21b), a reduction of the electropositive character on the tetrazine rings closest to the anions is evident. Particularly in the case of the neutral complex **4**, the decrease in the electropositive character of the tetrazine ring sandwiched between the two anions (Figure 22b, side view, upper ring) is more appreciable than in the other two tetrazine rings (Figure 22b, bottom view), due to two anions interacting with the upper tetrazine ring as compared to one anion per ring for the two lower rings (Figure 22b, side view). These observations strongly suggest a flow of electronic charge from the anions to the π-acidic rings (supported by previous reports that an increase in the aromaticity of the ring is observed upon interaction with the anion)[19h] and provide unambiguous computational evidence that favorable anion−π interactions are established between the anions and the bptz tetrazine rings in **3**, **4**, and **5b**. A notable observation about the dicationic unit $[Ag_2(bptz)_3]^{2+}$ in **4** is that one of the bptz ligands is more electropositive than the other two (Figure 22a, upper ring, side view); the more electropositive central tetrazine ring is the one closest to the $[AsF_6]^-$ anions in the crystal structure of $[Ag_2(bptz)_2(CH_3CN)_2][AsF_6]_2$ (Figure S7), which implies that stronger anion−π interactions are established with higher π-acidity rings.[20]

The lack of an appreciable electropositive character in the central pyridazine ring of bppn (Figures 17b,d and 18b,d) renders it less likely to participate in anion−π interactions as compared to bptz. The more electron-rich bppn central pyridazine ring is retained even after binding to Ag(I) ions, as indicated by the electrostatic potential map of the cationic unit $[Ag_4(bppn)_4]^{4+}$ (Figure 23a). The negligible difference in electropositive character between the central and outer rings of bppn in free bppn and in the cationic unit $[Ag_4(bppn)_4]^{4+}$ upon addition of the $[AsF_6]^-$ anions (Figure 23b) concurs with the preference of bppn for grid-type structures, as observed in the X-ray crystal structures of **6**−**9**, wherein the π−π stacking interactions of bppn are maximized (e.g., Figure 13a,b for **6**) at the expense of anion−π interactions. Since the change in electropositive character of the central rings of the bppn ligands in the cationic unit $[Ag_4(bppn)_4]^{4+}$ is negligible upon addition of the $[AsF_6]^-$ anions, the anion−π interactions present in complexes **6**−**9** are expected to be weaker than those in the bptz complexes **1**−**5b**. The fact that, for the neutral Ag(I)−bptz species studied herein, i.e., **3**, **4** (Figures 19, 22), the difference in the color intensities (and thus of the electron densities) between the central tetrazine ring of each complex and that of the corresponding dication (in the absence of anions) is greater than the corresponding color difference between the central pyridazine ring of the neutral Ag(I)−bppn complex **7** (Figure 23), and that of the corresponding cationic unit $[Ag_4(bppn)_4]^{4+}$, suggests that stronger anion−π interactions are established in the case of the bptz complexes.

The strength of the anion−π interactions has been correlated to the magnitude of the permanent quadrupole moment (Q_{zz} = 10.70, −4.922, and −7.99 Buckingham for *s*-tetrazine, pyridazine, and benzene, respectively)[80] and the molecular polarizability (*ab initio* calculations on the *s*-tetrazine ring with F^- ions demonstrate the significant contribution of the polarization term to the total binding energy of the anion−π interaction, which is consistent with the high polarizability of the *s*-tetrazine ring, $\alpha_{\parallel}$ = 58.7 au[19f]) of the π-system.[19c,h,22] The larger quadrupole moment of the bptz central rings as compared to bppn results in stronger anion−π interactions for the bptz complexes, which is corroborated by the shorter F···central ring distances[26] as well as the presence of multiple anion−π interactions per anion[19m] in the bptz complexes **1**−**5b** (Table 2).

Conclusions

In summary, we have undertaken a tandem crystallographic and computational investigation of the effect of anion−π interactions on the preferred structural motifs of Ag(I) complexes containing π-acidic aromatic rings. The higher π-acidic character of the bptz tetrazine ring as compared to the more electron-rich bppn pyridazine ring, suggested by the electrostatic potential maps of the free ligands, renders bptz more likely to participate in anion−π rather than π−π interactions. This preference is reflected in the resulting structural motifs of the Ag(I)−bptz complexes (polymers, planar dinuclear, or propeller-type dinuclear, depending on the anion) versus grid-type structures for the Ag(I)−bppn compounds, regardless of the anion. In the Ag(I)−bptz compounds **1**−**5b**, multiple and shorter (thus stronger) anion−π interactions are established between the anions and the central tetrazine rings, whereas in the grids **6**−**9**, intramolecular π−π interactions are maximized at the expense of anion−π interactions. The solid-state evidence of stronger anion−π interactions in the bptz complexes is supported by the results of DFT calculations (B3LYP/6-311+G(d,p) and BP86/TZP). The electrostatic potential maps of the Ag(I)−bptz species of **3**, **4**, and **5b** suggest a flow of electronic charge from the anions to their proximal π-acidic rings and the establishment of anion−π interactions between the anions and the bptz tetrazine rings. On the other hand, the small difference in electropositive character between the central and outer rings of bppn in the free ligand and the cationic unit $[Ag_4(bppn)_4]^{4+}$ of the

(80) Doerksen, R. J.; Thakkar, A. J. *J. Phys. Chem.* **1999**, *103*, 10009.

grid-type complex **7** suggests relatively weak anion$-\pi$ interactions between the bppn central rings and the anions. Further studies on similar systems are underway to gain additional insight into the nature of anion$-\pi$ interactions with multiatomic anions, their interplay with $\pi-\pi$ interactions, and the extent to which they influence the outcome of self-assembly reactions.

Acknowledgment. Prof. F. P. Gabbaï is acknowledged for helpful discussions. K.R.D. gratefully acknowledges the Robert A. Welch Foundation and the National Science Foundation for a PI Grant (CHE-9906583) as well as for a grant to purchase the CCD X-ray equipment (CHE-9807975). The NMR instrumentation was funded by NSF (CHE-0077917). Use of the TAMU/LBMS Applications Laboratory (Laboratory of Biological Mass Spectroscopy) is acknowledged. We also thank the Supercomputing Facility and the Laboratory for Molecular Simulation at Texas A&M University for providing software and computer time.

Supporting Information Available: Crystallographic data for **1**−**4**, **5a**, **5b**, and **6**−**9** (CIF files). Figure S1, packing diagram of $\{[Ag(bptz)][PF_6]\}_\infty$ (**1**) in the *ab* plane; Figure S2, thermal ellipsoid plot of $[Ag_2(bptz)_2(CH_3CN)][AsF_6]_2$ (**3**); Figure S3, packing diagram of $[Ag_2(bptz)_2(CH_3CN)_2][AsF_6]_2$ **(3)** in the *bc* plane; Figure S4, fragment of the structure of $[Ag_2(bptz)_2(CH_3CN)_2][AsF_6]_2$ **(3)** depicting the shortest contacts between the $[AsF_6]^-$ anions and the tetrazine rings; Figure S5, thermal ellipsoid plot of $[Ag_2(bptz)_3][AsF_6]_2$ (**4**); Figure S6, packing diagram of $[Ag_2(bptz)_3][AsF_6]_2$ (**4**) in the *ab* plane; Figure S7, fragment of the $Ag_2(bptz)_3][AsF_6]_2$ (**4**) structure depicting the shortest contacts between the $[AsF_6]^-$ anions and the tetrazine rings; Figure S8, thermal ellipsoid plot of the dicationic unit $\{[Ag_4(bppn)_4][AsF_6]_2\}^{2+}$ in **7**; Figure S9, thermal ellipsoid plot of the dicationic unit $\{[Ag_4(bppn)_4][SbF_6]_2\}^{2+}$ in **8**; Figure S10, packing diagram of **6**; Figure S11, ESI-MS spectrum of $[Ag_2(bptz)_3][AsF_6]_2$ (**4**); full author lists for refs 64 and 68a. This material is available free of charge via the Internet at http://pubs.acs.org. CCDC depository numbers: **1**, CCDC-252223; **2**, CCDC-252669; **3**, CCDC-280800; **4**, CCDC-280801 and -229435; **5a**, CCDC-233336; **5b**, CCDC-233335; **6**, CCDC-280802; **7**, CCDC-247745; **8**, CCDC-247012; **9**, CCDC-280803.

JA0606273